1   **Tissue specific targeting of DNA nanodevices in a multicellular living organism.**

2   Kasturi Chakraborty[1,2], Sunaina Surana[1,2], Simona Martin[1,2], Jihad Aburas[3], Sandrine

3   Moutel[4], Franck Perez[4], Sandhya P. Koushika[5], Paschalis Kratsios[2,3,*] and Yamuna

4   Krishnan[1,2,*]

5   *[1]Department of Chemistry, The University of Chicago, Chicago IL 60637*

6   *[2]Grossman Institute of Neuroscience, Quantitative Biology and Human Behavior, The*

7   *University of Chicago, Chicago IL 60637*

8   *[3]Department of Neurobiology, The University of Chicago, Chicago IL 60637*

9   *[4]Dynamics of Intracellular Organization Laboratory, Institut Curie, PSL Research University,*

10   *Sorbonne Université, Centre National de la Recherche Scientifique, UMR 144, Paris, France*

11   *[5]Department of Biological Sciences, Tata Institute of Fundamental Research, Mumbai, India*

12

13   **Abstract**

14   Nucleic acid nanodevices present great potential as agents for logic-based therapeutic

15   intervention as well as in basic biology. Often, however, the disease targets that need

16   corrective action are localized in specific organs and thus realizing the full potential of DNA

17   nanodevices also requires ways to target them to specific cell-types *in vivo*. Here we show that

18   by exploiting either endogenous or synthetic receptor-ligand interactions and by leveraging the

19   biological barriers presented by the organism, we can target extraneously introduced DNA

20   nanodevices to specific cell types in *C. elegans*, with sub-cellular precision. The amenability

21   of DNA nanostructures to tissue-specific targeting *in vivo* significantly expands their utility in

22   biomedical applications and discovery biology.

23

24   **Introduction**

25   DNA has proven to be a versatile molecular scaffold to build an array of programmable

26   synthetic nanoarchitectures due to its structural predictability(Seeman & Sleiman, 2017). The

27   specificity of Watson-Crick base pairing, its tuneable affinity, the well-defined structural

28   properties of the double helix and its modular nature make the DNA scaffold highly

29   engineerable. A wide array of functional DNA-based nanodevices have been deployed *in vivo*

30   both for quantitative chemical imaging and also as programmable carriers that deliver

31   encapsulated cargo upon receipt of a molecular cue(Chakraborty, Leung, & Krishnan, 2017;

32   Chakraborty, Veetil, Jaffrey, & Krishnan, 2016; Douglas, Bachelet, & Church, 2012; Jani, Zou,

33   Veetil, & Krishnan, 2020; Krishnan & Bathe, 2012; Lee et al., 2012; J. Li et al., 2011; Modi et

34   al., 2009; Narayanaswamy et al., 2019; Saha, Prakash, Halder, Chakraborty, & Krishnan,

35   2015; Sharma, Zaveri, Visweswariah, & Krishnan, 2014; Surana, Bhat, Koushika, & Krishnan,

36   2011; Thekkan et al., 2019; Veetil et al., 2017; Zhao et al., 2012). However, in most contexts,

37   the site for payload action ideally needs to be confined to the desired organ or tissue. Thus, if

38   DNA nanodevices can be targeted tissue-specifically in a live, multicellular organism, it would

39   significantly expand their potential utility in biomedicine and fundamental biology.

40   Nature solves the problem of transporting poorly permeable molecules across

41   membrane barriers, either releasing or enriching them tissue-specifically, by membrane

42   trafficking. DNA nanostructures are particularly amenable to endosomal trafficking, which has

43   in part, led to an array of synthetic DNA nanostructures being presently deployed in living

44   systems(Bujold, Lacroix, & Sleiman, 2018; Chakraborty et al., 2016; Krishnan, Zou, & Jani,

45   2020). Endosomal trafficking is ubiquitous: it regulates the internalisation, sorting and

46   intracellular transport of diverse cargo, and is pivotal to development, signalling and

47   homeostasis. The significance and impact of endocytosis in health and disease is underscored

48   by the observation that perturbations in endosomal trafficking are linked to multiple diseases,

49   including neurodegeneration, cancer and cardiovascular disease and further, distinct cell types

50   differ in their susceptibility to disease(Maxfield, 2014; Mellman & Yarden, 2013; Mukherjee,

51   Ghosh, & Maxfield, 1997). By leveraging membrane trafficking as well as taking advantage of

52   biological barriers present in the whole organism, we show that DNA nanodevices can be

53   targeted tissue-specifically and with organelle-level precision in the nematode *Caenorhabditis*

54   *elegans*.

55   Most studies that use DNA nanostructures as reporters or payload carriers describe

56   their functionality primarily in cultured cells that express scavenger receptors for which DNA is

57   the natural ligand(J. Li et al., 2011; Modi et al., 2009). *In vivo* studies in multicellular organisms

58   have also exploited scavenger receptor-mediated endocytosis to target DNA architectures to

59   phagocytic cells such as coelomocytes in *C. elegans(Surana et al., 2011)* or microglia in *D.*

60   *rerio(Veetil et al., 2020)* (**Figure 1a**). However, since most cells and tissues do not

61   endogenously express, scavenger receptors, targeting DNA nanostructures to such cell types

62   *in vivo* remains challenging. In cultured cells, this problem is circumvented by exploiting

63   naturally occurring receptor-ligand interactions. The natural ligand is chemically conjugated to

64   a DNA nanodevice, which then binds its cognate receptor on the cell surface and gets

65   internalized and transported within the cell along the trafficking route adopted by the

66   receptor(Bhatia et al., 2016; Jani et al., 2020; Modi, Nizak, Surana, Halder, & Krishnan, 2013).

67   Alternately, a synthetic receptor-ligand interaction has been used where the receptor is a

68   sequence-specific, DNA-binding protein based on a single-chain variable fragment

69   (scFv)(Modi et al., 2013). When the scFv is fused to a trafficking protein such as furin, and the

70   chimera is expressed in cells, furin displays the synthetic scFv receptor on the cell surface.

71   Thus, DNA nanodevices with an scFv-binding sequence engage the scFv domain of the

72   chimera and get trafficked to specific organelles within the cell(Modi et al., 2013; Saminathan

73   et al., 2020). Despite these *in cellulo* demonstrations, there is still no evidence that DNA

74   nanostructures can be targeted to tissues lacking scavenger receptors in multicellular
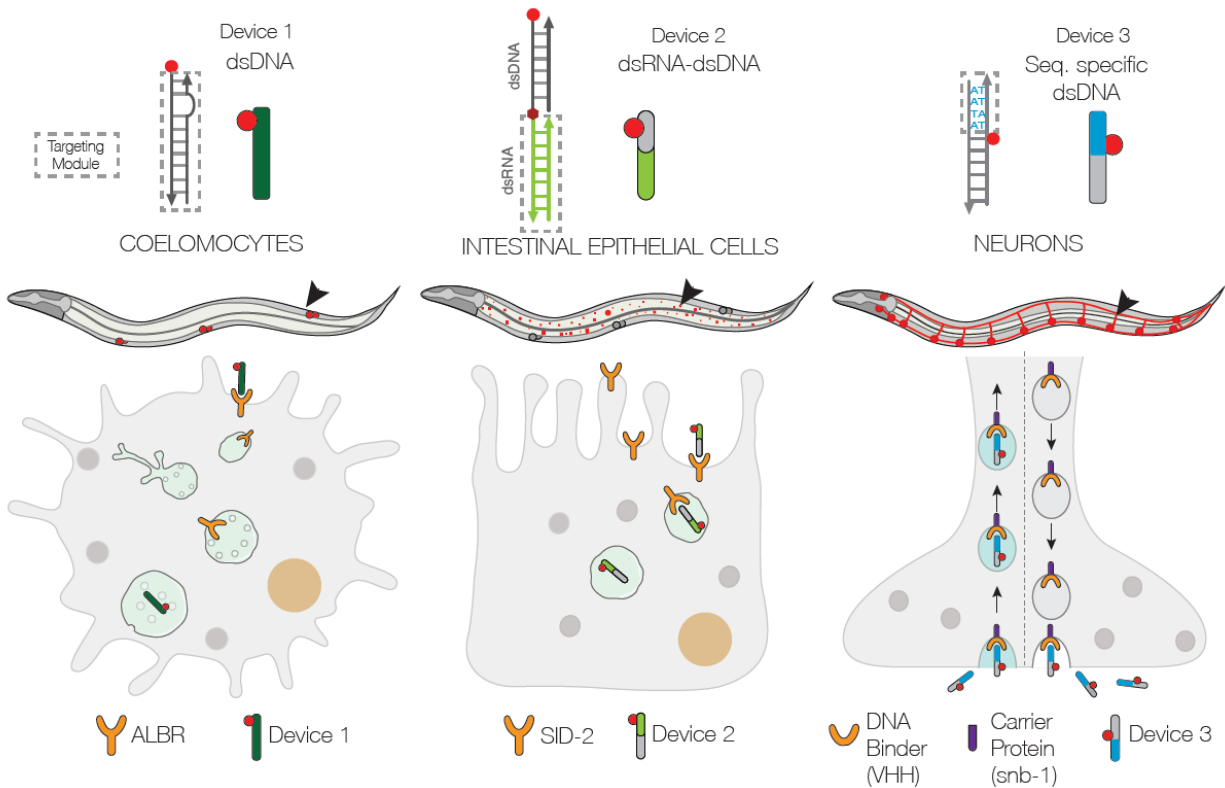
Figure 1: Schematic of strategies to target DNA devices to different cell types*:* (A) DNA nanodevices are intrinsically targeted to coelomocytes via the endogenously expressed scavenger receptors. (B) DNA nanodevices that display a dsRNA (green) domain are targeted to intestinal epithelial cells by engaging endogenously expressed SID-2 receptor. (C) DNA nanodevices are targeted selectively to those neurons that express a DNA-binding protein (V$_H$H) fused to synaptobrevin (*snb-1*). The DNA nanodevice has a sequence (blue) recognized specifically by V$_H$H.

75   organisms.

76   In this study, we demonstrate that DNA nanodevices can be targeted tissue-

77   specifically in the nematode *C. elegans* by leveraging both natural and synthetic receptors, on

78   the surface of different cell types. We have focussed on two tissues where endosomal

79   trafficking has been linked to critical physiological functions, namely, the intestine and the

80   nervous system. In the first instance, we exploit the presence of endogenous SID-2 receptors

81   on the intestine to target a DNA nanostructure along the endo-lysosomal pathway in intestinal

82   epithelial cells (**Figure 1b**). In the second, we present a generalizable route to target DNA

83   nanostructures to cells lacking either scavenger receptors or SID-2 receptors. Here, we use a

84   synthetic receptor, namely, a newly identified, recombinant, single-domain antibody (9E) which

85   tightly binds a specific 4-nt sequence of dsDNA. When 9E is fused to the synaptic vesicle

86   protein synaptobrevin-1 (SNB-1) and selectively expressed in neurons, the SNB-1::9E chimera

87   binds DNA nanodevices having the cognate 4-nt domain and localizes them in retrogradely-

88   moving endosomes in neurons (**Figure 1c**).

89   By leveraging the *C. elegans* amenability to transgenesis, we demonstrate the

90   molecular adaptability of this strategy. By expressing SNB-1::9E under promoters expressing

91   in specific sets of neurons, we show that DNA nanodevices can be targeted to retrogradely-

92   moving endosomes in specific neurons. We then demonstrate sub-cellular control over

93   targeting afforded by this synthetic system. We show that DNA nanodevices can be displayed

94   on the neuronal surface without invoking their entry into organelles. When 9E is genetically

95   fused to the transmembrane odorant receptor ODR-2 and expressed under a neuron-specific

96   promoter, it binds and positions a DNA nanodevice on the neuronal surface. The small size,

97   stability and pH-insensitivity of 9E makes this two-component system immediately suitable for

98   a multitude of DNA architectures bearing the cognate 4-nt sequence. Moreover, it offers a

99   versatile route to target diverse proteins or track endosomal transport trajectories in different

100   cell types *in vivo*, especially in model organisms amenable to transgenesis.

101

102   **Results and Discussion**

103   **Targeting DNA nanodevices to intestinal epithelial cells**

104   The intestine is one of the major organs of *C. elegans*, comprising a third of the total

105   somatic mass with twenty large epithelial cells positioned with bilateral symmetry, forming a

106   long tube around a lumen[(McGhee, 2007)](Altun & Hall, 2009). Intestinal epithelial cells (IECs)

107   contain prominent, birefringent gut granules that are known as lysosome-related organelles

108   (LROs). Distinguished by lysosomal markers(Coburn & Gems, 2013; Dell'Angelica, Mullins,

109   Caplan, & Bonifacino, 2000; Hermann et al., 2005), LROs play important roles in production

110   and storage of melanin, immune defence and neurological function(Huizing, Helip-Wooley,

111   Westbroek, Gunay-Aygun, & Gahl, 2008). We first sought to target a simple DNA nanodevice

112   comprising a 38-bp double stranded DNA (dsDNA) bearing a 5' Alexa 647 (A647), denoted

113   D^{38}, to label LROs in the intestinal epithelia (**Table 1**, **Supplementary Information**). We

114   reasoned that the biological barrier between the intestinal lumen and the pseudocoelom would

115   effectively preclude D^{38} from access to coelomocytes, as seen whenever DNA nanodevices

116   are microinjected in the pseudocoelom[Bhatia, Surana, Chakraborty, Koushika, & Krishnan, 2011; Surana et al., 2011].

117   We therefore utilized a liquid-feeding method to introduce 1 μM of D^{38} into the intestinal

118   lumen of one-day adult worms (M&M). We leveraged the high autofluorescence of LROs at

119   shorter wavelengths to provided regions of interest (ROIs) to evaluate the efficacy of D^{38}

120   uptake. The mean intensity corresponding to D^{38} uptake, compared to control mock-fed worms,

121   was very low, indicating low or no intrinsic targetability of DNA nanodevices to IECs. (**Figure**

122   **2a-b**). We therefore varied the size of the DNA nanodevice to test whether increasing the

123   number of base pairs (bp) and/or negative charges improved targeting, the sequences of which

124   are shown in **Table 1**, **Supplementary Information**. Using the same liquid-feeding method,

125   we repeated uptake experiments with 50 or 100 bp long dsDNA (D^{50} or D^{100}). Again, there was

126   no enhancement in nanodevice targeting to IECs (**Figure 2a**). This revealed DNA

127   nanostructures are not inherently targeted to cells in this tissue.

128   We then tested whether we could co-opt the RNA interference (RNAi) pathway in order

129   to target DNA-based probes to intestinal epithelia. Previous studies have shown that worms

130   are capable of endocytosing dsRNA localized in the acidic intestinal lumen, and that this is

131   effected by the membrane protein SID-2(Hunter et al., 2006; McEwan, Weisman, & Hunter,

132   2012; William M Winston, Sutherlin, Wright, Feinberg, & Hunter, 2007). We first tested the

133   uptake of dsRNAs either 50 bp or 100 bp long, denoted R^{50} or R^{100} respectively, based on

134   previous work suggesting this as the minimum length needed for effective internalisation by

135   SID-2 (**Figure 2a**)(McEwan et al., 2012)All dsRNAs carried a fluorescent Alexa647 label at

136   their 5' termini. Interestingly, when worms were liquid-fed either R^{100} or R^{50} we observed that

137   uptake efficiency by intestinal epithelia increased ~2-fold compared to their DNA analogues

138   (**Figure 2b**).

139   We therefore sought to test whether covalently attaching R^{100} or R^{50} to a DNA

140   nanodevice would promote nanodevice entry into the intestinal epithelia via the SID-2 receptor,

141   and potentially label LROs. Using click chemistry, we conjugated R^{100} to DNA nanodevices

142   D^{38}, D^{50} or D^{100} bearing Alexa647 labels to give chimeric RNA-DNA nanodevices denoted

143    $R^{100}D^{38}$, $R^{100}D^{50}$ and $R^{100}D^{100}$ respectively (**Figure 2c-d**, **Supplementary Fig 1**)(Jewett,

144   Sletten, & Bertozzi, 2010). When nematodes were liquid-fed the above chimeras and then

145   imaged, we found that overall, conjugating R^{100} to DNA nanodevices improved uptake of the

146   latter by intestinal epithelial cells. However, interestingly, we observed that the length of the
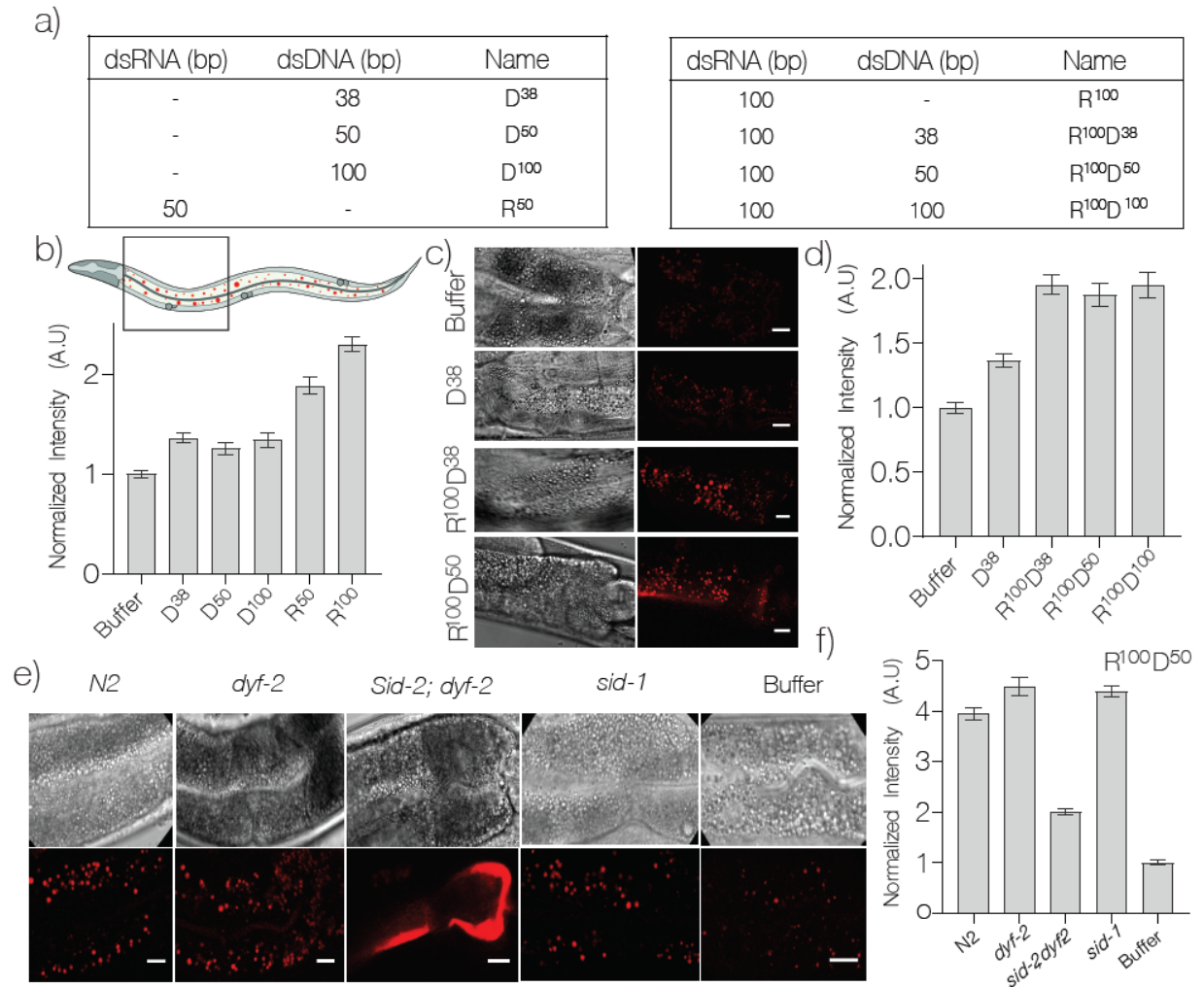
Figure 2: DNA nanodevices are targeted to intestinal epithelial cells. a) Table of the composition and length of the various Alexa-647 labeled DNA nanodevices used. B) Mean Alexa647 fluorescence intensity of corresponding to the uptake of the indicated nanodevice in *C. elegans* intestinal epithelial cells (IECs). c) Representative fluorescence and DIC images of IECs labelled with the indicated R^{100}-conjugated nanodevice quantified in d). e) Representative fluorescence images of IECs labelled with nanodevice $R^{100}D^{50}$ in the indicated genetic background quantified in g). Data represented as mean $\pm$ standard error of the mean of 10 worms, ~500 endosomes. The four IECs closest to the pharynx were considered for quantification. Scale bar = 10 μm

147   dsDNA scaffold had no significant effect on uptake efficiency (**Figure 2d**-**e**). Thus, it is possible

148   to target DNA nanodevices to intestinal epithelial cells using a DNA-RNA chimera.

149   Closer scrutiny revealed that $R^{100}D^n$ nanodevices internalized by intestinal epithelia

150   localized to lysosome related organelles (LROs), readily identified by their high

151   autofluorescence at low wavelengths(Soukas, Carr, & Ruvkun, 2013), as well as colocalization

152   with LAMP-1::GFP and GLO::1-GFP (**Supplementary Fig 1**)(**Schroeder et al., 2007; Soukas**

153   **et al., 2013**). In order to confirm the identity of the receptor responsible for the uptake of the

154   chimeric nanodevices into LROs, we repeated uptake assays in worms carrying mutant alleles

155   for *sid-1* and *sid-2*, two critical players of the RNAi pathway. Homozygous animals for the *sid-*

156   *1(qt9)* null allele are systemically resistant to RNAi(W M Winston, Molodowitch, & Hunter,

157   2002). The s*id-2* locus is embedded within an intron of another gene (*dyf-2*) and the only

158   available strong loss-of-function allele (*gk505*) for *sid-2* contains a 403 bp deletion, which

159   removes the first *sid-2* exon and the twelfth *dyf-2* exon. As a control for the *sid-2&dyf-2(gk505)*

160   strain, we used animals carrying the *dyf-2(gk678)* mutant allele that selectively disrupts the

161   *dyf-2* gene alone. Wild-type (N2 strain), *dyf-2, sid-1, and sid-2&dyf-2* worms were tested for

162   their ability to uptake $R^{100}D^{50}$ as previously described (**Figure 2d**-**e**). We found that uptake was

163   reduced in *sid-2&dyf-2* mutants, but not in *sid-1(qt9)*, *dyf-2(gk678)* or wild-type worms. Our

164   results are consistent with SID-2 being localized on the extracellular surface, acting as a

165   receptor that binds and endocytoses dsRNA, while SID-1 is resident in endosomes, where it

166   binds dsRNA cargo and transports it into the cytosol(Jose & Hunter, 2007; W. Li, Koutmou,

167   Leahy, & Li, 2015; McEwan et al., 2012). This implicates SID-2 as the receptor for nanodevice

168   internalisation and its subsequent trafficking to LROs in intestinal epithelial cells.

169

170   **Development of a DNA binding, recombinant camelid antibody**

171   *C. elegans* has proven to be a powerful model organism to study vesicular trafficking

172   in neurons, given its transparent body and simple nervous system(Hulme & Whitesides, 2011;

173   Teschendorf & Link, 2009). However, neurons do not express either scavenger receptors or

174   SID proteins, complicating the targeting of DNA nanodevices to these cell types. We therefore

175   developed a DNA-binding recombinant, camelid antibody (V_HH) as a synthetic receptor for

176   DNA nanodevices. This offers the advantage of tagging endogenously expressed proteins in

177   any cell of choice rather than ectopically expressing canonical DNA-binding proteins that could

178   have unknown biological effects. The small size of camelid antibodies, the ability to select them

179   by display technologies and tune their affinity, stability, and expression by molecular evolution

180   have led to a plethora of *in vivo* applications(Antibodies, Phage, & Technology, 1994). Camelid

181   antibodies lack a light chain altogether and the heavy chain domain itself is sufficient to form

182   the antigen binding pocket(Hamers-Casterman et al., 1993), leading to their utility in

183   therapeutics as well as cell biology(Harmsen & De Haard, 2007). They robustly maintain their

184   native conformations due to increased hydrophilicity and single domain nature and are much

185   more resistant to thermal and chemical denaturation(Dumoulin et al., 2002; Ewert, Cambillau,

186   Conrath, & Plückthun, 2002; Pérez et al., 2001; van der Linden et al., 1999).

187   We screened a recombinant llama antibody library to isolate high affinity candidates

188   that bind a specific DNA duplex and characterized the binding *in vitro*[5]. After a phage display

189   screen, we studied 160 potential binders and selected one of the highest affinity binders for

190   further evaluation for its affinity and specificity of binding. This binder, 9E, was further tested

191   for its expression, pH dependence and binding affinity. To date, V_HH recombinant antibodies

192   have been obtained using phage display against many classes of molecules, but not against

193   nucleic acids.

194   We therefore developed an assay to screen recombinant camelid antibodies by phage

195   display against a 41 bp dsDNA to obtain high-affinity, sequence-specific DNA binding

196   antibodies (**Materials and Methods**). The 41 bp dsDNA target was immobilized on streptavidin

197   coated magnetic beads via a 5′ biotinylated terminus and presented as the epitope to the V_HH

198   library (**Figure 3a**). Following standard procedure with the variations described above, three

199   rounds of progressive selection and amplification enriched for putative dsDNA binders. Next,

200   160 clones, were randomly selected, grown in 96 well plates and the corresponding phage

201   bound V_HH antibodies were expressed and screened for dsDNA binders. Nearly 70%

202   displayed DNA binding properties, of which 40 bound DNA regardless of whether it was

203   double- or single-stranded. Interestingly, 42 were found to show sequence specificity for the

204   dsDNA target and showed minimal binding to ssDNA of the same sequence or dsDNA with a

205   different sequence. These 42 clones were taken forwards for further analysis (**Supplementary**

206   **Figure 2**).

207   To screen for the minimal dsDNA motif recognized by each of the selected V_HH

208   antibody clones, ELISA was performed against a set of immobilized dsDNAs. These

209   corresponded to the full 41-mer dsDNA target and three shorter dsDNA regions R_1, R_2 and R_M

210   on the target (**Figure 3b**). Region R_1 corresponded to a 17 bp region at the 3′ terminus of the

211   biotinylated ssDNA oligonucleotide (nucleotides in red and blue font), R_2 corresponded to a 17

212   bp region on the 5' end of the oligonucleotide (nucleotides in green font), while R_M

213   corresponded to a 17 bp overlapping the 5′ end of R_1 and the 3′ of R_2 shown in italics. Of the

214   42-dsDNA binding V_HH antibodies tested, nearly 80% specifically bound region R_1, albeit with

215   varying affinities (**Supplementary Figure 3**).

216   To pinpoint the epitope on the 17-bp region R_1, partial duplexes were tested covering this

217   region with a sliding window of 4 bp from the 3' end of the biotinylated oligonucleotide to form

218   dsDNAs R_3 and R_6 (**Figure 3b**). This strategy ensured that the epitope could be narrowed

219   down to at least 4 bp. ELISAs revealed that each of the 42 V_HH antibodies required only the

220   first 4 bp at the 3' end of region R_1 (ATAA, nucleotides in red) for binding (**Figure 3c**). When
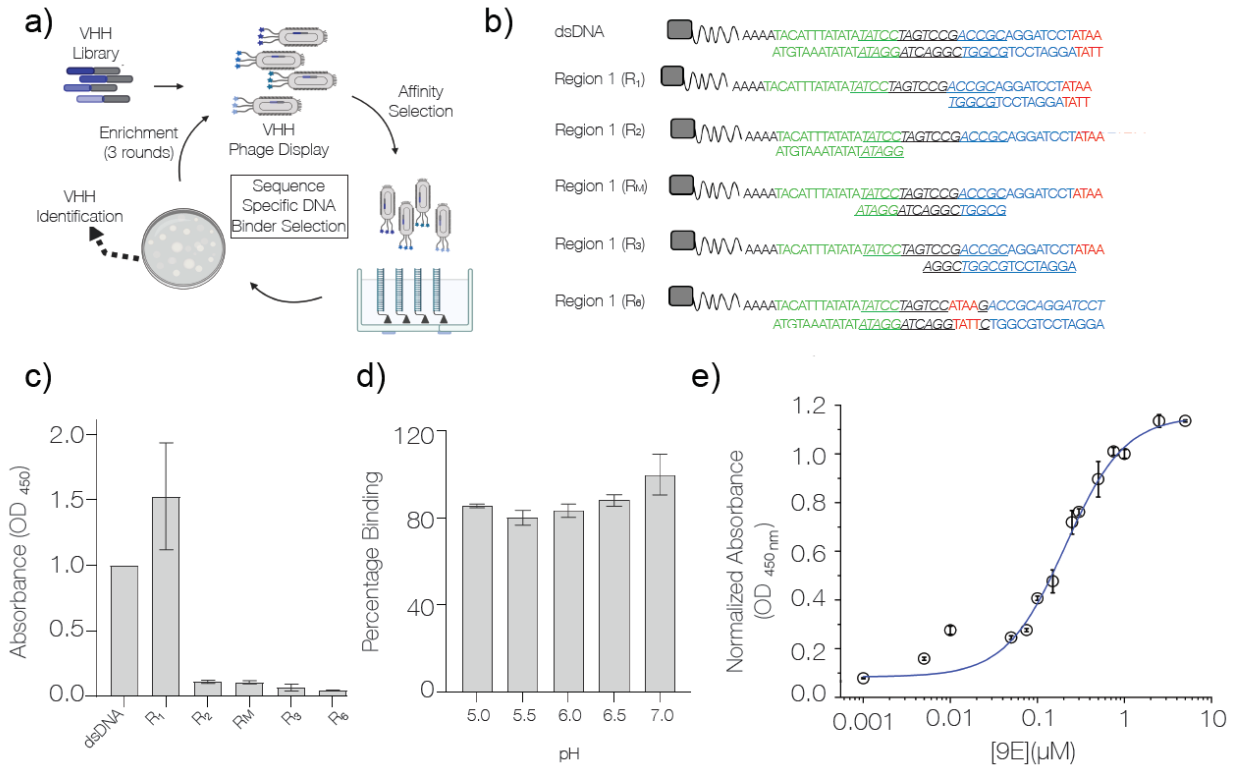
Figure3: Identification and characterization of a sequence-specific DNA-binding recombinant antibody 9E. a) Schematic of phage display screen to identify DNA binders using a camelid antibody (V$_H$H) library b) Sequence of the various dsDNA epitopes used to pinpoint the dsDNA sequence bound by the recombinant antibody, 9E. The tested regions are R1 (blue and red), R2 (green), an overlapping region RM (italicized and underlined), R3 (region R1 frame-shifted by a window of 4 nts) and R6 (4-nt motif in red, present in the middle of the DNA duplex). Biotin (grey square) was incorporated to immobilize the DNA epitopes on streptavidin-coated magnetic beads. c) Binding efficiencies of the recombinant antibody 9E with the indicated dsDNA constructs as determined by ELISA. d) Effect of pH on binding efficiency of 9E with dsDNA as determined by ELISA. e) The relative binding constant of 9E and dsDNA epitope in solution. Serial dilutions of the purified protein were added to a fixed amount of immobilized dsDNA (25 pmoles). All experiments were performed in triplicate and the data is represented as mean ± s.e.m.

221 this 4 bp sequence is present not at the terminus, but in the middle of the dsDNA duplex, as

222 in R_6, it was no longer a ligand for any of the 42 V_HH antibodies. This clearly demonstrated

223 that the minimal binding epitope for all 42 V_HH antibodies isolated was a terminal d(ATAA)

224 motif (**Supplementary Figure 3**). Furthermore, since endocytic events are accompanied by

225 lumenal pH changes, it is crucial to test whether binding between the V_HH antibody to its

226 cognate DNA epitope is pH-independent. From a pH-dependent ELISA screen we identified

227 that the V_HH 9E was disrupted the least of all by acidification, demonstrating ~82% binding

228 even at pH 5.0. (**Figure 3d, Supplementary Figure 4**). Finally, based on ELISA, we estimated

229 that the relative binding affinity of V_HH 9E to its target epitope was ~200 nM (**Figure 3e,**

230 **Materials and Methods**). Cumulatively, our findings show that the recombinant camelid

231 antibody V_HH 9E binds with high specificity to a 3' terminal, d(ATAA) region (**Supplementary**

232 **Figure 5**).

233

234 **Pan-neuronal expression of the SNB-1::9E chimera in *C. elegans***

235   Next, we tested whether DNA nanodevices could be targeted to neuronal endosomes

236 by genetically fusing 9E, the DNA-binding V_HH antibody identified above, with a protein such

237 as synaptobrevin (SNB-1), that is expressed in neurons and undergoes endosomal trafficking.

238 Our choice of synaptobrevin as a carrier protein was guided by it being an integral membrane

239 protein present in multiple copies in synaptic vesicles(Dittman & Ryan, 2009). It has a low

240 molecular weight (~16 kDa) and its N-terminal cytoplasmic domain interacts with target

241 membrane SNARE (t-SNARE) proteins to facilitate neurotransmitter exocytosis, while its C-

242 terminus has a hydrophobic patch that anchors it to vesicular membranes. The C-terminus

243 ends in a short tail which extends into the vesicular lumen and is exposed to the synaptic cleft

244 during exocytosis(Hanson, Heuser, & Jahn, 1997; Südhof, 1995). Upon their fusion with the

245 plasma membrane at the synaptic cleft, synaptic vesicles undergo recycling via the endosomal

246 pathway(Rizzoli, 2014). Furthermore, fusing GFP (~27 kDa) to the C-terminus of SNB-

247 1(Murthy, Bhat, & Koushika, 2011; Nonet, 1999), does not perturb SNB-1 localization or

248 function(Nonet, 1999) (**Figure 1c**).

249   Therefore, we reasoned that neuronal expression of an SNB-1::9E fusion protein would

250 lead to the 15 kDa V_HH domain being displayed in the synaptic cleft upon neurotransmitter

251 release. Thus, if DNA nanodevices bearing a terminal d(ATAA) motif were present in the

252 pseudocoelom, they could bind the V_HH domain (blue) of the chimera at the synaptic cleft and

253 get trafficked retrogradely along the endosomal pathway (**Scheme 1**). We therefore generated

254 transgenic *C. elegans* animals, denoted *Psnb-1:snb-1::9E* worms, that express the SNB-1::9E

255 chimera in all neurons under the control of the *snb-1* promoter (p*snb-1*)(Stefanakis, Carrera,

256 & Hobert, 2015), including an *unc-54* 3' UTR for efficient translation (**Figure 4a-b,**

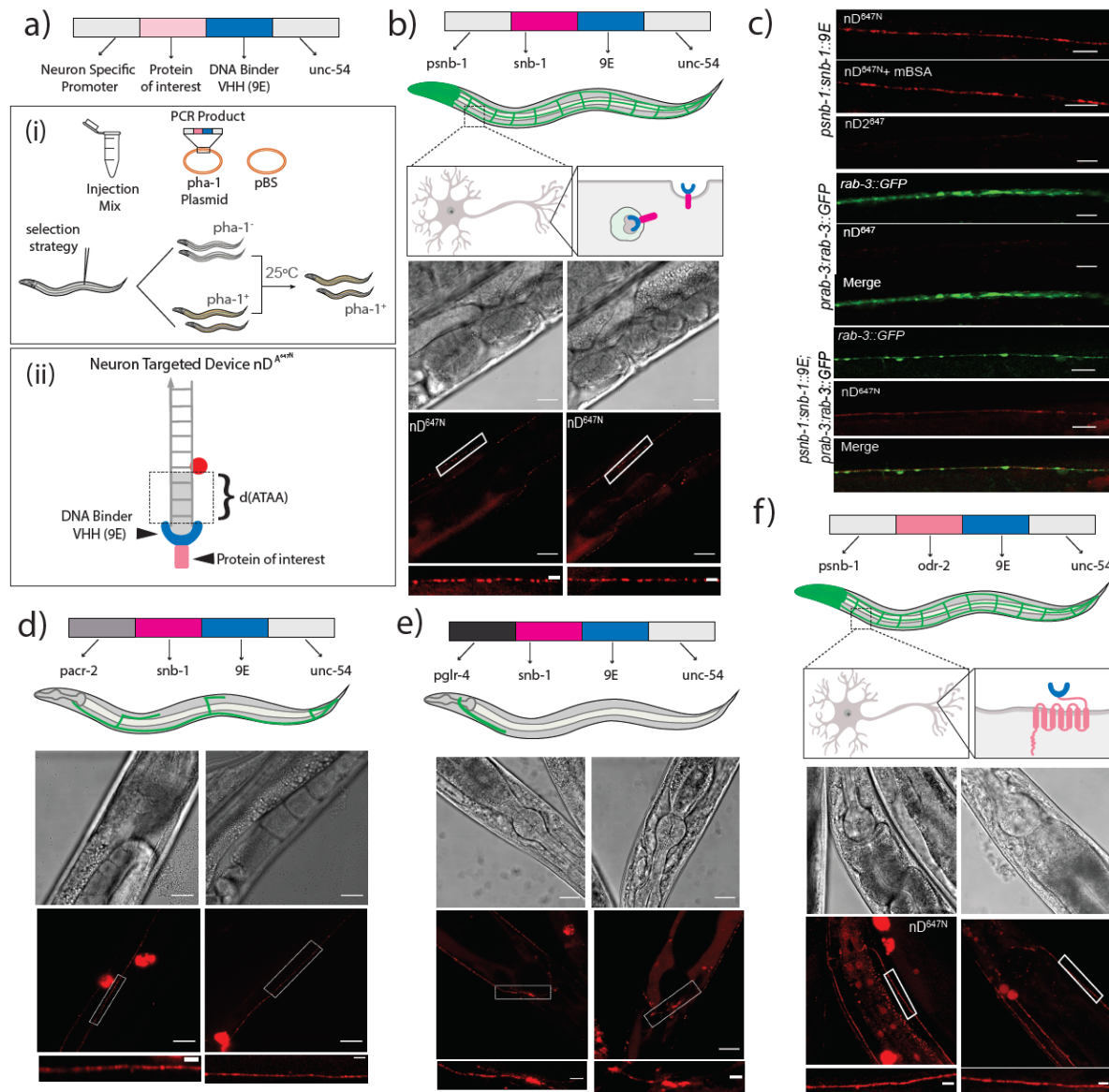257 **Supplementary Figure 6**). Into these worms we injected the DNA nanodevice D[38] (1 µM)

Figure 4: Targeting DNA nanodevices to neurons a) Schematic of the constructs used to make transgenics i) Strategy to select transgenics based on *pha-1+* worms ii) Schematic of neuron targetable DNA nanodevice nD^{A647} bound to its synthetic receptor, 9E, fused to the protein of interest. b) Schematic of nanodevice uptake into neurons of *psnb-1:snb-1::9E* worms. Brightfield and fluorescence images of *C. elegans* neurons labeled with nD^{A647}. c) Representative fluorescence images of i) neurons in *psnb1:snb-1::9E* worms injected with nD^{A647} in the presence or absence of mBSA and $nD2^{A647}$ lacking the 3' terminal d(ATAA) ii) neurons in *prab-3::gfp::rab-3* and iii) *prab-3::gfp::rab-3* ; *psnb1:snb-1::9E* expressing *C. elegans* injected with nD^{A647}. nD^{A647} can be targeted to neuronal subsets. d) nD^{A647} labels cholinergic neurons in *pacr-2:snb-1::9E* and glutamergic neurons in e) *pglr-4:snb-1::9E* expressing *C. elegans*. nD^{A647} can be targeted via the labeling cassette to other proteins cell-specifically. f) Images of neurons in *psnb1::odr-2::9E* expressing animals labeled with nD^{A647}.. In all images, the white boxedregion is shown in the zoomed image below. Scale: 20 µm; Inset: 5 µm.

258 modified to display a terminal d(ATAA) motif and an Atto 647N fluorophore, now denoted

259 nD^{A647}, into the pseudocoelom and imaged the worms after 30 min. We observed several

260 punctate structures, linearly arranged along the worm's body strongly resembling neuronal

261 synapses along the *C. elegans* dorsal and ventral nerve cords (**Figure 4b**).

262 To test whether the nanodevices were in fact labelling neurons and synapses, we performed

263 a series of colocalization experiments using transgenic *C. elegans* animals carrying different

264 neuronal and synaptic markers. The strain *otIs355 [rab-3p::2xNLS::tagRFP]* expresses

265 nuclear RFP pan-neuronally, whereas *otIs45 [unc-119p::GFP]* expresses cytosolic GFP pan-

266 neuronally (**Supplementary Figure 7)**(*Altun-Gultekin et al., 2001; Nguyen et al., 2016)*. The

267 *jsIs682 [rab-3p::gfp::rab-3]* strain expresses GFP::RAB-3 in most neurons, which is localized

268 primarily to synaptic regions (**Supplementary Figure 7)(Mahoney et al., 2006)**.

269 Hermaphrodites carrying the *Psnb-1:SNB-1::9E* transgene were crossed with each of the

270 aforementioned reporter strains (**Supplementary Figure 6)**. When 500 nM nD^{A647} was injected

271 into *jsIs682 [rab-3p::GFP::RAB-3]; Psnb-1:SNB-1::9E* worms, we found that nD^{A647N} labelling

272 coincides with RAB-3:GFP, confirming synaptic labelling. Interestingly, nD^{A647N} containing

273 puncta do not exclusively colocalize with RAB-3:GFP positive puncta within the same axon.

274 This suggests that in addition to the synaptic regions of neurons, nD^{A647N} might be labelling

275 retrogradely trafficking endosomal compartments or synaptic vesicles that are being recycled.

276 Similar colocalization experiments of nD^{A647} with other neuronal markers such as *otIs355 [rab-*

277 *3p::2xNLS::tagRFP]* and *otIs45 [unc-119p::GFP]* further confirmed that nD^{A647N} indeed labeled

278 neurons (**Supplementary Figure 7**).

279 Normally when DNA nanodevices are introduced into the pseudocoelom, they are

280 taken up by scavenger receptors present on coelomocytes(Chakraborty et al., 2017; Dan,

281 Veetil, Chakraborty, & Krishnan, 2019; Narayanaswamy et al., 2019; Surana et al., 2011; Veetil

282 et al., 2017). A key characteristic of nanodevice uptake via this pathway is that uptake is easily

283 abolished in the presence of 10 equivalent molar excess of maleylated BSA, as the latter

284 competes for scavenger receptors due to its anionic nature(Haberland & Fogelman, 1985).

285 Importantly, even in the presence of 10 equivalents excess of maleylated BSA, neuronal

286 labelling of *psnb-1:snb-1::9E* worms with nD^{A647} was not affected (**Figure 4c-i**). This indicates

287 that nD^{A647} uptake into neurons does not occur via scavenger receptors. When the terminal

288 d(ATAA) motif in nD^{A647} was removed to give a DNA nanodevice denoted nD2^{A647}, we observed

289 no such neuronal labelling (**Figure 4c-ii).** These results show that DNA nanodevices can be

290 targeted to neurons in worms only if the former incorporate a d(ATAA) motif, and if the latter

291 express the SNB-1::9E chimera in neurons.

292

293 **Targeting DNA nanodevices with cellular and subcellular precision**

294   To assess the precision over targeting using our method, we sought to localize DNA

295   nanodevices in endosomes of specific neuron types. We therefore expressed the SNB-1::9E

296   chimera under two different neuronal promoters. We focused on the cholinergic subset of

297   motor neurons since acetylcholine is the most broadly used neurotransmitter in the nematode

298   nervous system(Pereira et al., 2015). Cholinergic motor neurons in the ventral nerve cord are

299   divided into six classes: DA, DB, AS, VA, VB, and VC classes(Kerk, Kratsios, Hart, Mourao, &

300   Hobert, 2017). Since the acetylcholine receptor subunit ACR-2 is expressed in four of the six

301   classes of cholinergic motor neurons (DA, DB, VA, VB), we used the ACR-2 promoter region

302   to target these subsets of neurons(Kratsios, Stolfi, Levine, & Hobert, 2011). Transgenic *Pacr-*

303   *2::snb-1::9E* worms were generated using the previously described *pha-1* strategy (**Figure**

304   **4a**)(Granato, Schnabel, & Schnabel, 1994). When nD^{A647} (1 μM) was introduced into the

305   pseudocoelom of these nematodes, we observed that it localized in several, linearly arranged

306   punctate structures resembling synapses and/or neuronal endosomes, around the mid-section

307   of the worm body corresponding to the axons of the VA and VB neurons of the ventral nerve

308   cord (**Figure 4d**). The DA and DB neurons extend their axons to the dorsal nerve cord and

309   form synapse with dorsal muscle. However, we did not observe any labelling with nD^{A647} in the

310   dorsal nerve cord of *Pacr-2::SNB-1::9E* worms. Thus, our strategy selectively labels VA and

311   VB neurons over DA and DB classes of neurons. Such selective labelling could arise from the

312   differential cell surface levels of SNB-1::9E in VA and VB neurons, or greater accessibility of

313   their synapses to cargo in the pseudocoelom, or both.

314   Next, we targeted head neurons and a distinct set of cholinergic motor neurons, namely

315   the SAB class, located proximal to the pharynx that innervates the head muscles. In order to

316   target nD^{A647} to these neurons, we chose the promoter of the glutamate receptor family protein

317   GLR-4(Feng et al., 2006), since this protein is known to be expressed in the head neurons and

318   the SAB, VB and DA9 neurons(Brockie, Madsen, Zheng, Mellem, & Maricq, 2001; "glr-4 (gene)

319   - WormBase : Nematode Information Resource," n.d.; Hills, Brockie, & Maricq, 2004; Kratsios

320   et al., 2015; Rothaug et al., 2014). When nD^{A647N} (1 μM) was introduced into the pseudocoelom

321   of these nematodes, we observed that it localized in punctate structures arranged around the

322   pharynx, corresponding to the putative synapses of head neurons expressing *glr-4*, and ventral

323   neuromuscular synapses belonging to the SAB and VB neurons (**Figure 4e**). Again, just as in

324   the previous case of the DA and DB neurons, the DA9 neurons at the tail of the worm did not

325   show labelling, revealing that this method led to the preferential labelling of SAB and VB

326   neurons. Taken together, our results show that DNA nanodevices can be targeted to synapses

327   and/or retrogradely trafficking endosomes of specific neuron types expressing SNB-1::9E.

328   We then tested whether our method provides sub-cellular level precision in terms of

329   targeting individual neurons. Therefore, we tested whether we could target a DNA nanodevice

330   to neurons, and yet not allow neuronal entry, thereby keeping the DNA nanodevice

331 immobilized on the neuronal surface. We therefore genetically fused 9E to the ODR-2 protein

332 and expressed it under the pan-neuronal p*snb-1* promoter (**Figure 4f**). ODR-2 is a GPI-

333 anchored membrane-associated signalling protein that plays important roles in nematode

334 chemotaxis(Chou, Bargmann, & Sengupta, 2001). ODR-2 is highly expressed in sensory

335 neurons, motor neurons and interneurons, and is particularly enriched in axons(Gottschalk &

336 Schafer, 2006). Using the *pha-1* selection strategy described earlier, we obtained transgenics

337 stably expressing the ODR-2::9E chimera (**Figure 4a**). When these transgenics were injected

338 with nD^{A647N} (1 μM), we observed that in all worms, the DNA nanodevice labels neurons

339 corresponding to the ventral and the dorsal nerve cords (**Figure 4f**). In these transgenics, a

340 near-uniform pattern of plasma membrane labelling was observed that is reminiscent of ODR-

341 2 staining(Chou et al., 2001), and is in stark contrast to the punctate labelling that was

342 observed in p*snb-1::snb-1::9E* worms (**Figure 4b**). Taken together, our experiments show that

343 the synthetic receptor-ligand strategy shown here is generalizable to cell-surface membrane

344 proteins and can be used to label specific membrane domains and/or endosomal

345 compartments across neurons *in vivo*. Additionally, this design is applicable to a range of

346 functional DNA nanostructures provided they harbour a d(ATAA) tag, opening up new avenues

347 for the cell-specific application of DNA nanodevices in biological systems.

348

349 **Conclusion**

350 Endocytosis and endosome trafficking are complex processes, regulating many critical

351 cellular functions and therefore play pivotal roles in tissue-specific physiology and pathology.

352 Our knowledge of subcellular dynamics and organization of endocytic and recycling pathways

353 stems largely from investigations in cultured cellular systems. However, *in vivo*, endocytosis in

354 single cells and their functional outcomes are sculpted by molecular interactions with their

355 neighbouring cells, occurring in the presence of multiple biochemical cues originating from

356 other tissues. Thus, the ability to study endocytic pathways *in vivo*, at the single cell level and

357 in their native context, would illuminate our understanding of this core cellular process at the

358 whole organism level.

359 There is now a rich repertoire of investigative tools based on DNA nanodevices that

360 either probe or manipulate endosomal trafficking pathways(Krishnan et al., 2020). However,

361 in order to tap the full potential of DNA-based nanodevices *in vivo*, it is essential to develop

362 strategies for precise targeting to specific tissues. Here, we leverage both endogenous as well

363 as synthetic nucleic acid-binding receptors to specifically target simple DNA nanodevices to

364 two kinds of tissues: intestinal epithelial cells and neurons in *C. elegans*.

365 Our results show that, unlike what has been observed for coelomocytes(Chakraborty

366 et al., 2017; Dan et al., 2019; Narayanaswamy et al., 2019; Surana et al., 2011; Veetil et al.,

367 2017), simply introducing DNA nanodevices into the worm intestine and circumventing the

368   relevant biological barrier, does not lead to nanodevice targeting to intestinal epithelial cells.

369   This is due to the lack of an appropriate intestinal epithelial cell surface receptor for DNA.

370   However, by exploiting the endogenous dsRNA receptor SID-2 in intestinal epithelial cells, we

371   could target DNA nanodevices to these cells. We achieved this by conjugating a dsRNA

372   domain to DNA nanodevices, where the dsRNA domain engaged the SID-2 receptor such that

373   the DNA nanodevice underwent receptor-mediated endocytosis and was subsequently

374   trafficked to lysosome related organelles (LRO). Furthermore, since mutations in the *sid-2*

375   gene, but not *sid-1*, abrogated DNA nanodevice uptake, we could pinpoint that nanodevice

376   targeting occurs via the endogenous SID-2 receptor. Our results show that DNA nanodevices

377   can be targeted tissue-specifically by exploiting relevant endogenously expressed cell-surface

378   receptors and displaying the cognate ligand on the DNA nanodevice. Should new knowledge

379   of cell type-specific nucleic acid receptors, this strategy could be used to expand the targeting

380   of DNA nanodevices to other classes of cells.

381   In the absence of such knowledge, we have developed a synthetic receptor-ligand

382   strategy to target DNA nanodevices in a generalisable way so that it can be adapted to a

383   variety of cellular and molecular contexts *in vivo*. We therefore identified a sequence-specific,

384   DNA-binding recombinant camelid antibody, denoted 9E, by phage display. 9E binds a specific

385   4-nt sequence, namely d(ATAA) when it is present at the 3' end of the DNA nanodevice with

386   high affinity (~200 nM), irrespective of the environmental pH.

387   By fusing 9E to proteins that are expressed on the target cell under appropriate tissue-

388   specific promoters, we can target DNA nanodevices with cellular and sub-cellular level

389   precision. For example, since SNB-1 is ubiquitously expressed in all neurons, we expressed a

390   SNB-1::9E fusion protein under the pan-neuronal promoter p*snb-1* and targeted a DNA

391   nanodevice displaying the 3' terminal d(ATAA) sequence, specifically to neurons. Interestingly,

392   nanodevices labelled endosomes not only at the synapses but all along the axon within the

393   relevant neurons. Neuronal targeting required both, SNB-1 fused to the 9E antibody and the

394   DNA nanodevice to have the 3' d(ATAA) sequence. This established that cell-specific targeting

395   was contingent upon the interaction between the synthetic receptor and its cognate DNA

396   epitope. DNA nanodevices could be targeted to specific sub-sets of neurons by expressing the

397   SNB-1::9E chimera under promoters of genes expressed in specific neuronal classes. Thus,

398   when SNB-1::9E was expressed under p*acr-2* or p*glr-4* promoters(Feng et al., 2006; Kratsios

399   et al., 2015, 2011), DNA nanodevices were internalized by cholinergic ventral cord neurons or

400   SAB head motor neurons respectively.

401   We showed that targeting of DNA nanodevices could be achieved with sub-cellular

402   level precision using this strategy. Fusing 9E to the transmembrane odorant receptor, ODR-2,

403   which does not undergo significant endocytosis(Chou et al., 2001), enabled the immobilization

404   of a DNA nanodevice at the neuronal surface, rather than being endocytosed into intracellular

405   vesicles. This suggests that DNA nanodevices may be localized with subcellular precision

406   using a synthetic receptor and cognate ligand strategy *in vivo*.

407   To interrogate organelle dynamics and function *in vivo*, the development of robust

408   technologies with molecular specificity that enables access to discrete cell types is critical. The

409   modular system described here has the capability to interface with and harness, the power of

410   nucleic acid nanotechnology to probe and program specific tissues *in vivo***.** These targeting

411   strategies open up an array of possible applications where DNA nanodevices can be readily

412   applied in the multicellular context, and positions DNA nanodevices to deliver key insights into

413   complex biological phenomena.

414

422

423   **Author Contribution:** SS, KC, SPK, PK and YK designed the project. SS, SM, FP and YK

424   developed and characterized the recombinant 9E. KC and SM made constructs for transgenic

425   development. KC, JA and PK developed all new transgenics. KC developed all the DNA

426   nanodevices, performed biochemical assays, worm imaging and analysis. KC and YK

427   analyzed the data. KC, SS and YK wrote the paper. All authors discussed the results and gave

428   inputs on the manuscript.

429

430   **Competing interests:** The authors declare no competing interests.

431

432   **Data availability**

433   The data that support the plots within this paper and other finding of this study are available

434   from the corresponding author upon reasonable request.

435

436 **Bibliography**

437 Altun, Z. F., & Hall, D. H. (2009). Alimentary system, intestine. . *WormAtlas*. Retrieved from
438   http://doi:10.3908/wormatlas.1.4

439 Altun-Gultekin, Z., Andachi, Y., Tsalik, E. L., Pilgrim, D., Kohara, Y., & Hobert, O. (2001). A
440   regulatory cascade of three homeobox genes, ceh-10, ttx-3 and ceh-23, controls cell
441   fate specification of a defined interneuron class in C. elegans. *Development*, *128*(11),
442   1951–1969.

443 Antibodies, M., Phage, B. Y., & Technology, D. (1994). MAKING ANTIBODIES BY PHAGE.

444 Bhatia, D., Arumugam, S., Nasilowski, M., Joshi, H., Wunder, C., Chambon, V., … Krishnan,
445   Y. (2016). Quantum dot-loaded monofunctionalized DNA icosahedra for single-
446   particle tracking of endocytic pathways. *Nature Nanotechnology*, *11*(12), 1112–1119.
447   doi:10.1038/nnano.2016.150

448 Bhatia, D., Surana, S., Chakraborty, S., Koushika, S. P., & Krishnan, Y. (2011). A synthetic
449   icosahedral DNA-based host-cargo complex for functional in vivo imaging. *Nature*
450   *Communications*, *2*, 339. doi:10.1038/ncomms1337

451 Brockie, P. J., Madsen, D. M., Zheng, Y., Mellem, J., & Maricq, A. V. (2001). Differential
452   expression of glutamate receptor subunits in the nervous system of Caenorhabditis
453   elegans and their regulation by the homeodomain protein UNC-42. *The Journal of*
454   *Neuroscience*, *21*(5), 1510–1522.

455 Bujold, K. E., Lacroix, A., & Sleiman, H. F. (2018). DNA Nanostructures at the Interface with
456   Biology. *Chem*, *4*(3), 495–521. doi:10.1016/j.chempr.2018.02.005

457 Chakraborty, K., Leung, K., & Krishnan, Y. (2017). High lumenal chloride in the lysosome is
458   critical for lysosome function. *eLife*, *6*, e28862. doi:10.7554/eLife.28862

459 Chakraborty, K., Veetil, A. T., Jaffrey, S. R., & Krishnan, Y. (2016). Nucleic Acid-Based
460   Nanodevices in Biological Imaging. *Annual Review of Biochemistry*, *85*, 349–373.
461   doi:10.1146/annurev-biochem-060815-014244

462 Chou, J. H., Bargmann, C. I., & Sengupta, P. (2001). The Caenorhabditis elegans odr-2 gene
463   encodes a novel Ly-6-related protein required for olfaction. *Genetics*, *157*(1), 211–
464   224.

465 Coburn, C., & Gems, D. (2013). The mysterious case of the C. elegans gut granule: death
466   fluorescence, anthranilic acid and the kynurenine pathway. *Frontiers in genetics*, *4*,
467   151. doi:10.3389/fgene.2013.00151

468 Dan, K., Veetil, A. T., Chakraborty, K., & Krishnan, Y. (2019). DNA nanodevices map
469   enzymatic activity in organelles. *Nature Nanotechnology*, *14*(3), 252–259.
470   doi:10.1038/s41565-019-0365-6

471 Dell'Angelica, E. C., Mullins, C., Caplan, S., & Bonifacino, J. S. (2000). Lysosome-related
472   organelles. *The FASEB Journal*, *14*(10), 1265–1278. doi:10.1096/fasebj.14.10.1265

473 Dittman, J., & Ryan, T. A. (2009). Molecular circuitry of endocytosis at nerve terminals.
474   *Annual Review of Cell and Developmental Biology*, *25*, 133–160.
475   doi:10.1146/annurev.cellbio.042308.113302

476 Douglas, S. M., Bachelet, I., & Church, G. M. (2012). A logic-gated nanorobot for targeted
477   transport of molecular payloads. *Science*, *335*(6070), 831–834.
478   doi:10.1126/science.1214081

479 Dumoulin, M., Conrath, K., Van Meirhaeghe, A., Meersman, F., Heremans, K., Frenken, L.
480   G. J., … Matagne, A. (2002). Single-domain antibody fragments with high
481   conformational stability. *Protein Science*, *11*(3), 500–515. doi:10.1110/ps.34602

482 Ewert, S., Cambillau, C., Conrath, K., & Plückthun, A. (2002). Biophysical properties of
483   camelid V(HH) domains compared to those of human V(H)3 domains. *Biochemistry*,
484   *41*(11), 3628–3636. doi:10.1021/bi011239a

485 Feng, Z., Li, W., Ward, A., Piggott, B. J., Larkspur, E. R., Sternberg, P. W., & Xu, X. Z. S.
486   (2006). A C. elegans model of nicotine-dependent behavior: regulation by TRP-family
487   channels. *Cell*, *127*(3), 621–633. doi:10.1016/j.cell.2006.09.035

488 glr-4 (gene) - WormBase : Nematode Information Resource. (n.d.). Retrieved January 7,
489   2021, from https://wormbase.org/species/c_elegans/gene/WBGene00001615#0-9f31-
490   10

491 Gottschalk, A., & Schafer, W. R. (2006). Visualization of integral and peripheral cell surface
492   proteins in live Caenorhabditis elegans. *Journal of Neuroscience Methods*, *154*(1-2),
493   68–79. doi:10.1016/j.jneumeth.2005.11.016
494 Granato, M., Schnabel, H., & Schnabel, R. (1994). pha-1, a selectable marker for gene
495   transfer in C. elegans. *Nucleic Acids Research*, *22*(9), 1762–1763.
496   doi:10.1093/nar/22.9.1762
497 Haberland, M. E., & Fogelman, A. M. (1985). Scavenger receptor-mediated recognition of
498   maleyl bovine plasma albumin and the demaleylated protein in human monocyte
499   macrophages. *Proceedings of the National Academy of Sciences of the United States*
500   *of America*, *82*(9), 2693–2697.
501 Hamers-Casterman, C., Atarhouch, T., Muyldermans, S., Robinson, G., Hamers, C., Songa,
502   E. B., … Hamers, R. (1993). Naturally occurring antibodies devoid of light chains.
503   *Nature*, *363*(6428), 446–448. doi:10.1038/363446a0
504 Hanson, P. I., Heuser, J. E., & Jahn, R. (1997). Neurotransmitter release - four years of
505   SNARE complexes. *Current Opinion in Neurobiology*, *7*(3), 310–315.
506   doi:10.1016/S0959-4388(97)80057-8
507 Harmsen, M. M., & De Haard, H. J. (2007). Properties, production, and applications of
508   camelid single-domain antibody fragments. *Applied Microbiology and Biotechnology*,
509   *77*(1), 13–22. doi:10.1007/s00253-007-1142-2
510 Hermann, G. J., Schroeder, L. K., Hieb, C. A., Kershner, A. M., Rabbitts, B. M., Fonarev, P.,
511   … Priess, J. R. (2005). Genetic analysis of lysosomal trafficking in Caenorhabditis
512   elegans. *Molecular Biology of the Cell*, *16*(7), 3273–3288. doi:10.1091/mbc.E05-01-
513   0060
514 Hills, T., Brockie, P. J., & Maricq, A. V. (2004). Dopamine and glutamate control area-
515   restricted search behavior in Caenorhabditis elegans. *The Journal of Neuroscience*,
516   *24*(5), 1217–1225. doi:10.1523/JNEUROSCI.1569-03.2004
517 Huizing, M., Helip-Wooley, A., Westbroek, W., Gunay-Aygun, M., & Gahl, W. A. (2008).
518   Disorders of lysosome-related organelle biogenesis: clinical and molecular genetics.
519   *Annual Review of Genomics and Human Genetics*, *9*, 359–386.
520   doi:10.1146/annurev.genom.9.081307.164303
521 Hulme, S. E., & Whitesides, G. M. (2011). Chemistry and the worm: Caenorhabditis elegans
522   as a platform for integrating chemical and biological research. *Angewandte Chemie*,
523   *50*(21), 4774–4807. doi:10.1002/anie.201005461
524 Hunter, C. P., Winston, W. M., Molodowitch, C., Feinberg, E. H., Shih, J., Sutherlin, M., …
525   Fitzgerald, M. C. (2006). Systemic RNAi in Caenorhabditis elegans. *Cold Spring*
526   *Harbor Symposia on Quantitative Biology*, *71*, 95–100. doi:10.1101/sqb.2006.71.060
527 Jani, M. S., Zou, J., Veetil, A. T., & Krishnan, Y. (2020). A DNA-based fluorescent probe
528   maps NOS3 activity with subcellular spatial resolution. *Nature Chemical Biology*,
529   *16*(6), 660–666. doi:10.1038/s41589-020-0491-3
530 Jewett, J. C., Sletten, E. M., & Bertozzi, C. R. (2010). Rapid Cu-free click chemistry with
531   readily synthesized biarylazacyclooctynones. *Journal of the American Chemical*
532   *Society*, *132*(11), 3688–3690. doi:10.1021/ja100014q
533 Jose, A. M., & Hunter, C. P. (2007). Transport of sequence-specific RNA interference
534   information between cells. *Annual Review of Genetics*, *41*, 305–330.
535   doi:10.1146/annurev.genet.41.110306.130216
536 Kerk, S. Y., Kratsios, P., Hart, M., Mourao, R., & Hobert, O. (2017). Diversification of
537   c. elegans motor neuron identity via selective effector gene repression. *Neuron*,
538   *93*(1), 80–98. doi:10.1016/j.neuron.2016.11.036
539 Kratsios, P., Pinan-Lucarré, B., Kerk, S. Y., Weinreb, A., Bessereau, J.-L., & Hobert, O.
540   (2015). Transcriptional coordination of synaptogenesis and neurotransmitter
541   signaling. *Current Biology*, *25*(10), 1282–1295. doi:10.1016/j.cub.2015.03.028
542 Kratsios, P., Stolfi, A., Levine, M., & Hobert, O. (2011). Coordinated regulation of cholinergic
543   motor neuron traits through a conserved terminal selector gene. *Nature*
544   *Neuroscience*, *15*(2), 205–214. doi:10.1038/nn.2989

545 Krishnan, Y., & Bathe, M. (2012). Designer nucleic acids to probe and program the cell.
546   *Trends in Cell Biology*, *22*(12), 624–633. doi:10.1016/j.tcb.2012.10.001
547 Krishnan, Y., Zou, J., & Jani, M. S. (2020). Quantitative imaging of biochemistry in situ and at
548   the nanoscale. *ACS central science*, *6*(11), 1938–1954.
549   doi:10.1021/acscentsci.0c01076
550 Lee, H., Lytton-Jean, A. K. R., Chen, Y., Love, K. T., Park, A. I., Karagiannis, E. D., …
551   Anderson, D. G. (2012). Molecularly self-assembled nucleic acid nanoparticles for
552   targeted in vivo siRNA delivery. *Nature Nanotechnology*, *7*(6), 389–393.
553   doi:10.1038/nnano.2012.73
554 Li, J., Pei, H., Zhu, B., Liang, L., Wei, M., He, Y., … Fan, C. (2011). Self-assembled
555   multivalent DNA nanostructures for noninvasive intracellular delivery of
556   immunostimulatory CpG oligonucleotides. *ACS Nano*, *5*(11), 8783–8789.
557   doi:10.1021/nn202774x
558 Li, W., Koutmou, K. S., Leahy, D. J., & Li, M. (2015). Systemic RNA Interference Deficiency-
559   1 (SID-1) Extracellular Domain Selectively Binds Long Double-stranded RNA and Is
560   Required for RNA Transport by SID-1. *The Journal of Biological Chemistry*, *290*(31),
561   18904–18913. doi:10.1074/jbc.M115.658864
562 Mahoney, T. R., Liu, Q., Itoh, T., Luo, S., Hadwiger, G., Vincent, R., … Nonet, M. L. (2006).
563   Regulation of synaptic transmission by RAB-3 and RAB-27 in Caenorhabditis
564   elegans. *Molecular Biology of the Cell*, *17*(6), 2617–2625. doi:10.1091/mbc.E05-12-
565   1170
566 Maxfield, F. R. (2014). Role of endosomes and lysosomes in human disease. *Cold Spring
567   Harbor Perspectives in Biology*, *6*(5), a016931. doi:10.1101/cshperspect.a016931
568 McEwan, D. L., Weisman, A. S., & Hunter, C. P. (2012). Uptake of extracellular double-
569   stranded RNA by SID-2. *Molecular Cell*, *47*(5), 746–754.
570   doi:10.1016/j.molcel.2012.07.014
571 McGhee, J. D. (2007). The C. elegans intestine. *Wormbook: the Online Review of C.
572   Elegans Biology*, 1–36. doi:10.1895/wormbook.1.133.1
573 Mellman, I., & Yarden, Y. (2013). Endocytosis and cancer. *Cold Spring Harbor Perspectives
574   in Biology*, *5*(12), a016949. doi:10.1101/cshperspect.a016949
575 Modi, S., M G, S., Goswami, D., Gupta, G. D., Mayor, S., & Krishnan, Y. (2009). A DNA
576   nanomachine that maps spatial and temporal pH changes inside living cells. *Nature
577   Nanotechnology*, *4*(5), 325–330. doi:10.1038/nnano.2009.83
578 Modi, S., Nizak, C., Surana, S., Halder, S., & Krishnan, Y. (2013). Two DNA nanomachines
579   map pH changes along intersecting endocytic pathways inside the same cell. *Nature
580   Nanotechnology*, *8*(6), 459–467. doi:10.1038/nnano.2013.92
581 Mukherjee, S., Ghosh, R. N., & Maxfield, F. R. (1997). Endocytosis. *Physiological Reviews*,
582   *77*(3), 759–803. doi:10.1152/physrev.1997.77.3.759
583 Murthy, K., Bhat, J. M., & Koushika, S. P. (2011). In vivo imaging of retrogradely transported
584   synaptic vesicle proteins in Caenorhabditis elegans neurons. *Traffic*, *12*(1), 89–101.
585   doi:10.1111/j.1600-0854.2010.01127.x
586 Narayanaswamy, N., Chakraborty, K., Saminathan, A., Zeichner, E., Leung, K., Devany, J., &
587   Krishnan, Y. (2019). A pH-correctable, DNA-based fluorescent reporter for organellar
588   calcium. *Nature Methods*, *16*(1), 95–102. doi:10.1038/s41592-018-0232-7
589 Nguyen, J. P., Shipley, F. B., Linder, A. N., Plummer, G. S., Liu, M., Setru, S. U., … Leifer, A.
590   M. (2016). Whole-brain calcium imaging with cellular resolution in freely behaving
591   Caenorhabditis elegans. *Proceedings of the National Academy of Sciences of the
592   United States of America*, *113*(8), E1074–81. doi:10.1073/pnas.1507110112
593 Nonet, M. L. (1999). Visualization of synaptic specializations in live C. elegans with synaptic
594   vesicle protein-GFP fusions. *Journal of Neuroscience Methods*, *89*(1), 33–40.
595   doi:10.1016/s0165-0270(99)00031-x
596 Pereira, L., Kratsios, P., Serrano-Saiz, E., Sheftel, H., Mayo, A. E., Hall, D. H., … Hobert, O.
597   (2015). A cellular and regulatory map of the cholinergic nervous system of C.
598   elegans. *eLife*, *4*. doi:10.7554/eLife.12432

599 Pérez, J. M., Renisio, J. G., Prompers, J. J., van Platerink, C. J., Cambillau, C., Darbon, H.,
600   & Frenken, L. G. (2001). Thermal unfolding of a llama antibody fragment: a two-state
601   reversible process. *Biochemistry*, *40*(1), 74–83. doi:10.1021/bi0009082
602 Rizzoli, S. O. (2014). Synaptic vesicle recycling: steps and principles. *The EMBO Journal*,
603   *33*(8), 788–822. doi:10.1002/embj.201386357
604 Rothaug, M., Zunke, F., Mazzulli, J. R., Schweizer, M., Altmeppen, H., Lüllmann-Rauch, R.,
605   … Blanz, J. (2014). LIMP-2 expression is critical for β-glucocerebrosidase activity and
606   α-synuclein clearance. *Proceedings of the National Academy of Sciences of the
607   United States of America*, *111*(43), 15573–15578. doi:10.1073/pnas.1405700111
608 Saha, S., Prakash, V., Halder, S., Chakraborty, K., & Krishnan, Y. (2015). A pH-independent
609   DNA nanodevice for quantifying chloride transport in organelles of living cells. *Nature
610   Nanotechnology*, *10*(7), 645–651. doi:10.1038/nnano.2015.130
611 Saminathan, A., Devany, J., Veetil, A. T., Suresh, B., Pillai, K. S., Schwake, M., & Krishnan,
612   Y. (2020). A DNA-based voltmeter for organelles. *Nature Nanotechnology*.
613   doi:10.1038/s41565-020-00784-1
614 Schroeder, L. K., Kremer, S., Kramer, M. J., Currie, E., Kwan, E., Watts, J. L., … Hermann,
615   G. J. (2007). Function of the Caenorhabditis elegans ABC transporter PGP-2 in the
616   biogenesis of a lysosome-related fat storage organelle. *Molecular Biology of the Cell*,
617   *18*(3), 995–1008. doi:10.1091/mbc.e06-08-0685
618 Seeman, N. C., & Sleiman, H. F. (2017). DNA nanotechnology. *Nature Reviews Materials*,
619   *3*(1), 17068. doi:10.1038/natrevmats.2017.68
620 Sharma, S., Zaveri, A., Visweswariah, S. S., & Krishnan, Y. (2014). A fluorescent nucleic
621   acid nanodevice quantitatively images elevated cyclic adenosine monophosphate in
622   membrane-bound compartments. *Small (Germany)*, *10*(21), 4276–4280.
623   doi:10.1002/smll.201400833
624 Soukas, A. A., Carr, C. E., & Ruvkun, G. (2013). Genetic regulation of Caenorhabditis
625   elegans lysosome related organelle function. *PLoS Genetics*, *9*(10), e1003908.
626   doi:10.1371/journal.pgen.1003908
627 Stefanakis, N., Carrera, I., & Hobert, O. (2015). Regulatory Logic of Pan-Neuronal Gene
628   Expression in C. elegans. *Neuron*, *87*(4), 733–750. doi:10.1016/j.neuron.2015.07.031
629 Südhof, T. C. (1995). The synaptic vesicle cycle: a cascade of protein-protein interactions.
630   *Nature*, *375*(6533), 645–653. doi:10.1038/375645a0
631 Surana, S., Bhat, J. M., Koushika, S. P., & Krishnan, Y. (2011). An autonomous DNA
632   nanomachine maps spatiotemporal pH changes in a multicellular living organism.
633   *Nature Communications*, *2*, 340. doi:10.1038/ncomms1340
634 Teschendorf, D., & Link, C. D. (2009). What have worm models told us about the
635   mechanisms of neuronal dysfunction in human neurodegenerative diseases?
636   *Molecular Neurodegeneration*, *4*, 38. doi:10.1186/1750-1326-4-38
637 Thekkan, S., Jani, M. S., Cui, C., Dan, K., Zhou, G., Becker, L., & Krishnan, Y. (2019). A
638   DNA-based fluorescent reporter maps HOCl production in the maturing phagosome.
639   *Nature Chemical Biology*, *15*(12), 1165–1172. doi:10.1038/s41589-018-0176-3
640 van der Linden, R. H., Frenken, L. G., de Geus, B., Harmsen, M. M., Ruuls, R. C., Stok, W.,
641   … Verrips, C. T. (1999). Comparison of physical chemical properties of llama VHH
642   antibody fragments and mouse monoclonal antibodies. *Biochimica et Biophysica
643   Acta*, *1431*(1), 37–46. doi:10.1016/s0167-4838(99)00030-8
644 Veetil, A. T., Chakraborty, K., Xiao, K., Minter, M. R., Sisodia, S. S., & Krishnan, Y. (2017).
645   Cell-targetable DNA nanocapsules for spatiotemporal release of caged bioactive
646   small molecules. *Nature Nanotechnology*, *12*(12), 1183–1189.
647   doi:10.1038/nnano.2017.159
648 Veetil, A. T., Zou, J., Henderson, K. W., Jani, M. S., Shaik, S. M., Sisodia, S. S., … Krishnan,
649   Y. (2020). DNA-based fluorescent probes of NOS2 activity in live brains. *Proceedings
650   of the National Academy of Sciences of the United States of America*, *117*(26),
651   14694–14702. doi:10.1073/pnas.2003034117

652 Winston, W M, Molodowitch, C., & Hunter, C. P. (2002). Systemic RNAi in *C. elegans*
653   requires the putative transmembrane protein SID-1. *Science*, *295*(5564), 2456–2459.
654   doi:10.1126/science.1068836
655 Winston, William M, Sutherlin, M., Wright, A. J., Feinberg, E. H., & Hunter, C. P. (2007).
656   Caenorhabditis elegans SID-2 is required for environmental RNA interference.
657   *Proceedings of the National Academy of Sciences of the United States of America*,
658   *104*(25), 10565–10570. doi:10.1073/pnas.0611282104
659 Zhao, Y.-X., Shaw, A., Zeng, X., Benson, E., Nyström, A. M., & Högberg, B. (2012). DNA
660   origami delivery system for cancer therapy with tunable release properties. *ACS*
661   *Nano*, *6*(10), 8684–8691. doi:10.1021/nn3022662
662
663

Supplementary Information for:

Tissue specific targeting of DNA nanodevices in a multicellular living organism.

Kasturi Chakraborty[1,2], Sunaina Surana[1,2], Simona Martin[1,2], Jihad Aburas[3], Sandrine Moutel[4],

Franck Perez[4], Sandhya P. Koushika[5], Paschalis Kratsios[2,3,*] and Yamuna Krishnan[1,2,*]

[1]*Department of Chemistry, The University of Chicago, Chicago IL 60637*
[2]*Grossman Institute of Neuroscience, Quantitative Biology and Human Behavior, The University of Chicago, Chicago IL 60637*
[3]*Department of Neurobiology, The University of Chicago, Chicago IL 60637*
[4]*Dynamics of Intracellular Organization Laboratory, Institut Curie, PSL Research University, Sorbonne Université, Centre National de la Recherche Scientifique, UMR 144, Paris, France*
[5]*Department of Biological Sciences, Tata Institute of Fundamental Research, Mumbai, India*

Oligonucleotides All fluorescently labeled DNA oligonucleotides were HPLC-purified and obtained from IBA-GmBh (Germany) and IDT (Coralville, IA, USA). Unlabeled DNA oligonucleotides were purchased from IDT (Coralville, IA, USA). RNA was transcribed *in vitro* using a MEGAscript® T7 Kit (Invitrogen, USA). geneBlock fragements were obtained from IDT (Coralville, IA, USA)

Sequences of the various oligonucleotides used are listed below in Table 1.

Preparation of oligonucleotide samples All oligonucleotides were ethanol precipitated, dissolved in Milli-Q water, aliquoted as a 100 μM stock and stored at -20°C. Concentration of each oligonucleotide was measured using UV absorbance at 260 nm.

An intestinal epithelial cell targeting probe consist of an azido labelled RNA duplex conjugated to a DBCO containing fluorophore or DNA duplex via copper free click chemistry[1–3]. A PCR fragment of 100 bp or 50 bp template with a T7 promoter site obtained from a plasmid DNA was used as a template for *in vitro* transcription using protocols suggested by the manufacturer (MEGAscript® T7 Kit, Invitrogen, USA). The ability of T7 RP to incorporate different 5′-modified guanosine analogues was utilized in transcriptional priming to label and specifically conjugate the 5′-terminus of transcripts[4,5]. for incorporating a 5′-azide reactive group. In the IVT reaction, 5′-azido-5′-deoxy guanosine (5 '-N_3G) is added in fourfold excess over GTP to prime transcriptions [1]. RNA formation was confirmed by gel electrophoresis (PAGE) (Figure S1). The transcript with the 5 '-terminal azide (R-N_3) is subsequently used in click reactions with a fluorophore or DNA strand containing a dibenzocyclooctyl (DBCO) group. The click conjugation is performed in 10 mM sodium acetate buffer pH 5.5. This conjugated strand was then annealed to the corresponding complementary strands heating at 90°C for 5 min, and then slowly cooling to room temperature at 5°C per 15 min.

A sample of duplex DNA for screening of DNA binding V_HH was made by mixing the relevant DNA oligonucleotides in equimolar ratios, heating at 90°C for 5 min, and then slowly cooling to room temperature at 5°C per 15 min. This sample preparation was carried out with oligonucleotide concentrations of 5 μM, in phosphate buffered saline (PBS) of pH 7.3, in the presence of 100 mM KCl. Samples were then equilibrated at 4°C overnight. Samples were used within 7 days of annealing.

Selective oligonucleotides were phosphorylated at their 5' end by incubating them with T4 polynucleotide kinase (PNK; New England Biolabs, USA). 2 nmoles of the oligonucleotide were mixed with 2 μL of 10× PNK buffer, 2 μL of PNK (10 U/μL), 4 μL of 1 mM ATP and the volume

was made up to 20 µL. This reaction mix was incubated at 37˚C for 1 h. Post-incubation, the enzyme was inactivated by incubating the mixture at 75˚C for 15 min. The DNA was subsequently ethanol precipitated, re-suspended in Milli-Q water and quantified using UV absorbance. These were then used to prepare duplex DNA using the protocol mentioned above.

A sample of the neuronal targeting probe (nD^{A647N}) was made by mixing the DNA oligonucleotides nD and nD' in equimolar ratios, heating at 90°C for 5 min, and then slowly cooling to room temperature at 5°C per 15 min. This sample preparation was carried out with oligonucleotide concentrations of 5 µM, in 10 mM phosphate buffer of pH 7.4, in the presence of 100 mM KCl. Samples were then equilibrated at 4°C overnight.

Preparation of helper phages *Escherichia coli* strain TG1 grown in minimal media (M9 media) was inoculated 1:100 in 100 mL 2×TY media and grown till OD$_{600}$ reached 0.2. 200 µL of this culture was then transferred to tubes and infected with serial dilutions of 4×10^{11} M13KO7 helper phage (with a minimum ratio of 1 bacterium per 20 helper phages, GE Healthcare, USA) (10-10, 10^{-11}, 10^{-12}, 10^{-13}, 10^{-14}). The tube was quickly transferred to a 37°C water bath and incubated for 30 min without shaking. 3 mL of H-Top agar was heated to 42˚C and quickly poured to each tube. This was then poured on 2×TY plates and incubated overnight at 37˚C. The plaques obtained from each plate were inoculated in 3 mL of 2×TY and grown till optical density at 600 nm (OD$_{600}$) reaches 0.5. At this stage, the cultures were again infected with helper phage and incubated for 2 h at 37˚C with shaking. This was diluted in 500 mL of 2×TY media and incubated at 37˚C for 1 h, after which kanamycin was added to a final concentration of 50 µg/mL and the culture was incubated overnight at 37˚C. The overnight culture was centrifuged at 10800×g for 15 min and the supernatant was collected into a glass conical flask. This flask was transferred to ice and 100 mL ice cold polyethylene glycol/NaCl solution (30% PEG 8000 with 2.5 M NaCl) was added with constant shaking. The resulting mixture was kept on ice for 45 min. The solution became turbid and was centrifuged at 10800×g for 30 min and the supernatant was discarded. The phage precipitate was re-suspended in 6 mL PBS containing 30% glycerol. This was filtered using a 0.45 µm membrane filter (Merck Millipore, USA), aliquoted and stored at -80˚C.

Preparation of library A 250 µL aliquot of the glycerol stock library (4x10^{10} clones/mL) was inoculated in 250 mL of 2xTY containing 100 µg/mL of ampicillin (Sigma-Aldrich, USA) and 1% glucose. This was incubated at 37°C till the OD$_{600}$ reached 0.5. 25 mL (containing 10^{10} clones) of this culture was infected with an excess of helper phage M13KO7, with a minimum ratio of 1 bacterium per 20 helper phages. Care was taken that no pipetting or shaking was done. This was incubated for 30 min at 37˚C, without agitation, in a water bath. The infected bacteria were centrifuged for 20 min at 4200 rpm, the pellet was re-suspended in 500 mL of 2xTY with 100 µg/mL ampicillin and 50 µg/mL kanamycin without glucose, and incubated overnight at 30°C with shaking. The overnight culture was centrifuged at 10800×g at 4˚C for 10 min. 100 mL of ice cold PEG-NaCl solution was added to the supernatant of the centrifuged culture, such that the supernatant becomes cloudy. This was incubated for 1 h on ice at 4˚C. The mixture was centrifuged for 30 min at 10800×g at 4˚C to pellet the phages. The PEG/NaCl solution was aspirated off carefully without disturbing the pellet. The pellet was re-suspended in 40 mL Milli-Q water, after which 8 mL of PEG/NaCl was added. The solution was swirled for efficient but gentle mixing and then allowed to stand on ice at 4˚C for 20 min. The phages were centrifuged again at 10800×g for 30 min. The PEG/NaCl supernatant was carefully removed. The pellet containing a purified library of phages was re-suspended in 5 mL cold PBS and centrifuged again for 10 min at 13000 rpm at 4˚C to pellet cell debris and bacteria. This is used as input for the phage display screen. The rest is stored as aliquots at -80˚C.

Preparation of DNA conjugated magnetic beads 150 µL streptavidin-coupled magnetic Dynabeads (Invitrogen, USA) were washed 3 times in PBS supplemented with 0.1% Tween-20

(Sigma-Aldrich, USA) (PBST). After each wash, beads were collected using a magnet. 15 µL of the B-RO3-CELL duplex (oligonucleotides Biotin-R-CELL+O3-CELL) was added to the washed magnetic beads and the volume of the reaction made up to 500 µL with PBST, such that the final DNA concentration used for the screening is 50 nM. This was incubated on a rotator for 1 h. After 1 h, the DNA coated beads are washed in PBST 3 times and then suspended in 150 µL of PBS. For each round of selection, 50 µL aliquots of this DNA conjugated magnetic bead mix were used. The rest was stored at -20°C for future use.

Selection of dsDNA binders using phage display method The phage display screen was carried out using a previously described protocol 10, with some variations. Non-specific binders (in particular anti-streptavidin V_HHs) were removed from the library by incubating V_HHs displayed on the surface of phages with streptavidin-coated magnetic beads alone. 50 µL of streptavidin coated magnetic beads were mixed with 100 µL of the library (this input contains 1.1×10^{12} phages) and incubated for 30 min on a roller and another 30 min standing. Volume of this mix was made up to 1.5 mL with PBST supplemented with 0.6% non-fat milk (PBSTM). After 1 h, the beads containing streptavidin binders were pulled down using a magnet, while the supernatant containing the remainder of the library was added to 50 µL of the DNA coated magnetic beads. This mix was incubated on a roller for 30 min and then left standing for 1.5 h. After 2 h, the beads were pulled down using a magnet, the PBSTM was removed, 1 mL of fresh PBSTM was added and the beads were fully re-suspended. This mix was added to a 15 mL polypropylene tube, which was pre-blocked with PBSTM (2% non-fat milk), and the volume made up to 10 mL using PBST. The beads were collected using a magnet for 5 min, the PBST was removed and fresh PBST was added. This was repeated 20 times, with a change of polypropylene tube every 5 washes. After the last wash, 1 mL of 100 mM triethylamine (TEA) was added to re-suspend and dissociate the phages from the beads; this was transferred to a tube and rocked for 7 min, after which the beads were collected using a magnet. 500 µL of the supernatant was carefully added to a 500 µL of 1 M Tris-Cl (pH 7.4) to neutralize it; the remaining 500 µL was put back on the roller again for 7 min and the above steps were repeated. Finally, 200 µL of 1 M Tris-Cl was added to the polypropylene tube and kept separately.

Rescue and enrichment of possible DNA binders The rescue and amplification of selected phage was done by infecting *E. coli* TG-1 bacteria with eluted phage. 750 µL of the recovered phages were added to 9.25 mL of a TG1 culture (grown to an OD_{600} of 0.5 in 2×TY media with 1% glucose) and incubated at 37°C for 30 min in a water bath without agitation. Simultaneously, 4 mL of the same TG1 culture was added to the last polypropylene tube and the infection protocol was repeated. Both the cultures were pooled to get 14 mL of infected TG1 culture. Of this, 3 dilutions of 1 mL each were made, 10^{-1}, 10^{-2} and 10^{-3}, and two volumes of each, 10 µL and 100 µL, were spread on 2×TY plates containing 1% glucose and 100 µg/mL ampicillin. These plates were used for calculation of phage output after the first round of selection. The remaining culture was spun down at 3300 rpm for 10 min at RT. The pellet was re- suspended in 1.5 mL 2×TY, which was equally divided and plated on 3 large 2×TY plates containing 1% glucose and 100 µg/mL ampicillin. All plates were grown overnight at 37°C.

Colonies obtained on the large petri dishes were scraped off using 6 mL of 2×TY supplemented with 30% glycerol. This scraped culture constitutes the input for Round 2 of screening. An aliquot of this culture was added to 100 mL of 2×TY with 1% glucose and 100 µg/mL ampicillin, such that OD_{600} of the inoculated culture was 0.05. This was incubated at 37°C till OD_{600} reaches 0.5. 10 mL was aliquoted into a fresh tube, helper phages were added (bacteria: helper phage = 1:20; at OD_{600} = 0.5, a 10 mL culture of *E.coli* contains 4×109 bacteria) and the culture was incubated at 37°C in a water bath for 30 min without agitation. The culture was centrifuged at 3300 rpm for 10 min at RT, the pellet was re-suspended in 50 mL 2×TY with 100 µg/mL ampicillin and 50 µg/mL kanamycin (without glucose) and incubated overnight at 30°C.

40 mL of the overnight culture was centrifuged at 10800×g at 4˚C for 10 min. 8 mL of ice cold PEG-NaCl solution was added to the supernatant of the centrifuged culture, such that the supernatant becomes cloudy. This was incubated for 1 h on ice at 4˚C. The mixture was centrifuged for 10 min at 10800×g at 4˚C to pellet the phages. The PEG solution was aspirated off carefully without disturbing the pellet. The pellet was re-suspended in 2 mL cold PBS without introducing air bubbles. The phages were centrifuged again at 10800×g for 10 min. The supernatant was carefully removed. The pellet containing cell debris and bacteria was discarded, while the supernatant was used as input for Round 2 of selection. 500 µL dilutions of 10-9, 10-10 and 10-11 were also made with the recovered phages, introduced into TG1 bacteria (as described above) and spread on 2×TY plates containing 1% glucose and 100 µg/mL ampicillin to calculate input. This was done for 3 rounds of selection. Negative selection against streptavidin was done at each stage of selection to completely eliminate anti-streptavidin V_HHs.

After 3 rounds of screening, 80 clones each from Round 2 and 3 were selected for further characterization. Individual colonies were transferred to one well of a 2 mL deep 96-well plate (Greiner Bio-one, Germany) with 600 µL 2×TY containing 100 µg/mL ampicillin and 1% glucose, and grown overnight with shaking at 37°C. Glycerol was then added to a final concentration of 30% to make a master plate which was stored at -80°C.

ELISA using phages ELISA was performed using phages secreted in the media, each of which carries the V_HH fused to a coat protein. 600 µL of 2×TY with 100 µg/mL ampicillin and 1% glucose were added to each well of 2 mL deep 96 well plates, each of which was inoculated with 6 µL of the master stock. This was incubated for 2.5 h at 37°C with shaking, such that OD_{600} reaches 0.5. Helper phages were added to each well and the plates were incubated at 37°C without agitation. The plates were then centrifuged at 2500 rpm for 5 min. The supernatant was carefully aspirated off and the pellet re- suspended in 600 µL 2×TY containing 100 µg/mL ampicillin and 50 µg/mL kanamycin. The plates were incubated overnight at 30°C with agitation. The phages were recovered by centrifuging the cultures at 2800 rpm for 10 min at RT and pipetting the supernatant in fresh 96 well plates.

In order to perform the ELISA, 96 well ELISA plates (Nunc Maxisorp, Thermo Fisher Scientific, USA) were coated with 50 µL of 20 µg/mL avidin and incubated at RT for 2 h. The plates were flicked and washed once with PBS to remove excess avidin. 50 µL of biotinylated DNA at 50 nM concentration was immobilized by adding it to the wells and incubating at 4°C overnight. Excess DNA was removed by flicking the plates. The plates were blocked using 200 µL of and kept at RT for 1 h, after which it was removed by flicking. In a separate plate, 90 µL of phages were mixed with 20 µL of PBSTM, incubated at RT for 20 min and then 100 µL of this mix was added to the ELISA plate. The phages and DNA were allowed to bind for 2 h, after which the plates were flicked and washed 3 times each with PBST and PBS. 50 µL of anti-M13 antibody conjugated to horseradish peroxidise (HRP; GE Healthcare Life Sciences, USA) was added at a 1:5000 dilution and incubated for 40 min. The plates were flicked and washed 3 times with PBST and PBS. 100 µL of tetramethyl benzidine (TMB)/H_2O_2 (BD Biosciences, USA) was added to each well, and the reaction was stopped by addition of 100 µL of 2 N H_2SO_4. Binding was quantified by measuring absorbance at 450 nm using a Spectramax multi-mode plate reader (Molecular Devices, USA).

ELISA using secreted V_HHs ELISA was performed using V_HHs secreted in the media. 600 µL of 2×TY with 100 µg/mL ampicillin and 1% glucose was added to each well of 2 mL deep 96 well plates, each of which was inoculated with 6 µL of the master stock. This was incubated for 2 h at 37°C with shaking, after which 1 mM isopropyl thiogalactoside (IPTG) was added. The plates were then shifted to 30°C and incubated overnight. The cultures were centrifuged at 2800 rpm for 10 min at RT and the supernatant, which contains secreted V_HHs, was carefully transferred to a fresh 96 well plate. After this, standard ELISA, as outlined in Section IV.B.8.1 was carried out,

using mouse anti-Myc antibody (Sigma- Aldrich, USA) at a dilution of 1:1500 and goat anti-mouse antibody conjugated to HRP (Life Technologies, USA) at a dilution of 1:1000.

Characterization of sequence specificity Approximately 80 colonies each from Round 2 and Round 3 of selection were screened by ELISA against the dsDNA of choice (Biotin-R-CELL+O3-CELL). This screening was done using both phage and protein ELISA, as described above. In order to check the sequence specificity of the positive clones, V_HHs were subjected to another round of ELISA assay against various DNA epitopes. The epitopes used were ssDNA (Biotin-R-CELL, Biotin-O3-CELL), dsDNA (Biotin-R-CELL+O3-CELL), divergent dsDNA (Biotin-DS1-CELL+DS2-CELL) and various parts of the dsDNA (Biotin-R-CELL+R1-CELL, Biotin-R-CELL+RM-CELL, Biotin-R-CELL+R2-CELL, Biotin-R-CELL+R3-CELL, Biotin-R-CELL+R4-CELL, Biotin-R-CELL+R5-CELL). After immobilization of these targets, ELISA assay was carried out as mentioned above.

Sequencing of specific clones About 42 clones showing binding to dsDNA were chosen for sequencing. Individual clones were grown overnight and subjected to a plasmid DNA isolation using Nucleospin Plasmid Miniprep Kit (Macherey-Nagel GmbH, Germany). Sequencing was performed using a standard dideoxy sequencing method.

Expression and purification of V_HHs V_HH expression was performed in M9 minimal media (1× M9 salts, 2 mM $MgSO_4$, 1% glycerol, 0.1% casamino acids and 0.000005% thiamine). Selected V_HH was inoculated in 100 mL 2×TY supplemented with 100 µg/mL ampicillin and 1% glucose and grown overnight at 37°C. 5 ml of this culture was inoculated in 500 mL of M9 minimal media with 100 µg/mL ampicillin and grown at 37°C for 2 h. IPTG was added to a final concentration of 1 mM, after which the culture was shaken at 30°C for 16 h. Bacteria were centrifuged at 10000 rpm for 10 min. The supernatant containing secreted V_HHs was filtered using a 0.22 µm membrane filter to remove the remaining debris. The filtered media was then incubated with 2 mL of Talon Cobalt affinity resin (Clontech Laboratories Inc., USA) for 1 h at 4°C. Post-binding, the media with the resin was put into a funnel adapted onto a column, which was pre-washed with 20 mL of PBS, at 4°C. The flow through was collected and again passed through the column in order to collect all the metal beads with bound protein. This was done 3 times. Once all the beads were collected, they were washed again by passing 100 mL of PBS through the column. Non- specific binding to beads was abrogated using 1 mL 5 mM imidazole. The bound V_HH was then eluted using a gradient of imidazole concentrations, ranging from 50 mM to 250 mM. The first 9 fractions were run on a 12% SDS-PAGE to check the expression and elution of the protein.

Each eluted V_HH was further purified by removing imidazole using a 10 kDa Amicon ultra centrifugal filter (Merck Millipore, USA). Each fraction was added to the centrifugal filter and centrifuged for 10 min at 4°C for 14000 rpm. Volumes were then made up to 400 µL using PBS after each spin. This was repeated 10 times. Concentration of each fraction was measured using Bradford assay. Purified V_HH were stored at 4°C for short term and at - 20°C for long term.

pH dependent ELISA pH dependent ELISA to check pH sensitivity of the selected V_HH was performed using purified V_HH. The V_HH solution was divided into two pools and each pool was incubated with PBSTM of the desired pH for 20 min. This was then added to ELISA plates containing the immobilized DNA of choice. Standard ELISA, as described above, was then employed to assess binding.

Determination of V_HH binding affinities Affinity of selected V_HHs for their dsDNA epitopes was assessed using 3 formats, as described below. All data was analyzed using OriginPro 8.5 (OriginLab, USA).

i) Using serial dilutions of immobilized DNA Avidin coated 96-well plates were incubated with serial dilutions of the dsDNA antigen (10 nM - 5 µM), as described in Section IV.B.8. 250 nM of the protein was added and allowed to bind for 2 h. ELISA was then carried out as described above.

ii) Using serial dilutions of competitive DNA 500 nM of the biotinylated dsDNA antigen was mixed with serial dilutions of competitor non-biotinylated dsDNA (1 nM - 25 µM), to which 100 nM of protein was added. This mixture was allowed to incubate for 2 h at RT, after which it was added to avidin coated 96-well plates and further incubated for 2 h. ELISA was then performed.

iii) Using serial dilutions of purified V_HH Avidin coated 96-well plates were incubated and bound with 500 nM of the dsDNA antigen as described in Section IV.B.8. Serial dilutions of the protein (1 nM - 5 µM) were added and allowed to bind for 2 h. ELISA was then carried performed.

Electrophoretic mobility shift assay The required dsDNA constructs were annealed, as described above, at concentrations of 5 µM. A binding reaction was set up consisting of 1 µM DNA and 1 µM protein in PBS. Glycerol was added to a final concentration of 10% in order to minimize DNA-protein complex dissociation. DNA-protein complexes were allowed to form at RT for 2 h, after which 50 pmoles of DNA were loaded on an 8% native PAGE. The gel was run at 4°C using Tris-acetate-EDTA (TAE) buffer at 100 V. The DNA-protein complexes were visualized using ethidium bromide staining.

Plasmid vectors and construction of 9E fusions. PHA-1 plasmid (gift from Krastosis lab, University of Chicago) and pBluescript SK(-) (Agilent Technologies, USA) were used during construction of transgenic strains. PCR fragments containing promoters of choice, *snb-1* or *odr-2* and 9E were generated using standard cloning protocols. *psnb-1:odr-2* and *snb-1::9E* geneBlock fragments were obtained from IDT. *pglr-4, psnb-1, 9E* was cloned out of plasmids generated in house (*pglr-4*- Krastosis lab; *psnb-1* and 9E- Krishnan lab). *pacr-2 was* cloned out of genomic DNA isolated from wild type worms. All the PCR fragments had a *unc-54*- 3'UTR sequence on their 3' end for better expression in worms[6].

***C. elegans* methods and strains** Wild type strain used was the *Caenorhabditis elegans* isolate from Bristol (strain N2)[7]. Mutant strains used are VC1119 (*dyf-2&ZK520.2(gk505) III*), VC1521 (*dyf-2(gk678) III*), HC196 (*sid-1(qt9) V*). Other transgenics used for colocalization studies are as follows

1. *jsIs682* [p*rab-3::gfp::rab-3*][8,9] expresses GFP::RAB-3 in all neurons.
2. *otIs355* [*rab3p(prom1)::2xNLS::TagRFP*] which expresses RFP in the nucleus of all neurons[10]
3. *otIs45* [*unc-119::GFP*] which expresses GFP in the cytosol of all neurons[11]
4. *pwIs50* [*lmp-1::GFP + Cbr-unc-119(+)*] which expresses LMP-1::GFP a lysosomal marker[12].
5. *hjIs9* [*ges-1p::glo-1::GFP + unc-119(+)*] in which GFP is targeted to lysosome related organelles (LROs) in intestinal cells[13]

All strains were procured from the *Caenorhabditis* Genetics Centre (CGC; University of Minnesota, USA). Standard methods were followed for the maintenance of *C. elegans*.

Transgenic strains were created by co-injecting PCR fragment of the gene of interest and PHA-1 plasmid (20 ng/µl) as a selectable marker in *pha-1* mutants[14]. The PCR fragments used in this study were *psnb-1:snb-1::9E psnb-1:odr-2::9E; pglr-4:snb-1::9E* and *pacr-2:snb-1::9E.* Total concentration of injected DNA was 100 ng/µl, which was achieved using empty pBluescript SK(-) vector. Transgenic lines obtained were also maintained using standard protocols. *pha-1* mutants

are temperature sensitive embryonic lethal mutants which can grow at 15°C but not 25 °C[15]. Each line was characterized based on the survival at 25 °C.

Intestinal epithelia and neuron labelling Intestinal labeling was done by soaking worms in a 10 µL, 1 µM solution of intestine targeting probe at pH 5.0 for 2 hours. Worms were then washed in PBS and placed on OP50 plates for another hour before imaging. Worms were mounted on 2.0% agarose pads and anesthetized using 40 mM sodium azide in M9 buffer.

Neuronal labelling was done by injecting 500 nM of nD^{A647N}. Injections were performed, as previously described[16], in the dorsal side in the pseudocoelom, just opposite the vulva, of one-day old adult wild type hermaphrodites. Injected worms were mounted on 2.0% agarose pads and anesthetized either using 40 mM sodium azide or 1mM levimasole in M9 buffer. Neuronal labeling was examined after 30- 60 minutes of incubation at 22°C. Imaging of labelled neurons was carried out in at least 15 worms.

Co-localization experiments For gut colocalization experiments ~10 one-day adult transgenic worms were incubated in a solution of 1 µM $R^{100}D^{38}$ for two hours. Worms were then washed and incubated on OP50 plates for 1 hour for the clearing of the intestine lumen of excess sensor.

For neuronal co-localization experiments *psnb-1:snb-1::9E* were crossed with various transgenic lines containing fluorescently labelled neuronal markers. Briefly, L4 for hermaphrodite worms of various fluorescently labelled transgenic lines were crossed with N2 males and the male progeny containing a fluorescent label were selected for the next step. Fluorescently labeled male worms were crossed with *psnb-1:snb-1::9E* containing L4 hermaphrodites. 10-12 hermaphrodite progeny from this step were singled out at the L4 developmental stage based on the presence of a fluorescent marker. These worms were allowed to self-fertilize and 5 of their progenies were used to perform single worm PCRs to identify which plates contain worms with both 9E and the fluorescent neuronal markers. Single worm PCRs were performed using standard methods[17]. Briefly, 5 worms from each plate were placed into a tube containing 5µL of worm lysis buffer (WLB: 50 mM KCl, 10 mM Tris pH 8.3, 2.5 mM $MgCl_2$, 0.8% Tween-20, 0.01% Gelatin) and 100 µg/ml proteinase K. Worms are frozen at -80°C for at least one hour. The tube is immediately treated at 60°C for 60min after which proteinase K is inactivated by heating to 95°C for 15min. The PCR mix is then added directly to the digested heat inactivated sample. The PCR product was then confirmed by gel electrophoresis for 9E. Actin was used as a control. Plates which showed the presence of *psnb-1:snb-1::9E* were taken forward for injecting the DNA device similar to protocols mentioned above.

Worms were mounted on 2.0% agarose pads and anesthetized using either 40 mM sodium azide or 1 mM levimasole in M9 buffer and imaged on Leica TCS SP5 II STED laser scanning confocal microscope (Leica Microsystems, Inc., Buffalo Grove, IL, USA) in confocal mode.

Microscopy and image analysis Confocal images were captured with a Leica TCS SP5 II STED laser scanning confocal microscope (Leica Microsystems, Inc., Buffalo Grove, IL, USA) equipped with 63X, 1.4 NA, oil immersion objective. Alexa 488 was excited using an Argon ion laser for 488 nm excitation, Alexa 647 using He-Ne laser for 633 excitation. Images on the same day were acquired under the same acquisition settings. All the images were background subtracted prior to any image analysis, which was carried out using ImageJ ver.1.49d (NIH, USA).

Image analysis for quantification of uptake during intestinal labeling was done using custom MATLAB code. For each worm the most focused plane was manually selected in the Alexa 647 channel. To determine the location of the endosome first a low threshold was used to select the entire field. Only the area within the cell was subsequently considered for vesicle selection. Regions of interest corresponding to individual vesicle were selected in the Alexa 647 channel by

adaptive thresholding using Sauvola's method [18]. The initial selection was further refined by watershed segmentation and size filtering. After segmentation regions of interest were inspected in each image and selection errors were corrected manually. Using this we measured the mean fluorescence intensity for ~500 vesicles from ~10 animals and the background intensity corresponding to that field was subtracted.

**Table 1. Sequences of oligonucleotides employed in this study.**

| Name	Sequences 5'-3'
R1^{50}	GGA CTC TGG GGT TCG AAA TGA CCG ACC AAG CGA CGC CCA ACC TGC CAT CC
R2^{50}	GGA TGG CAG GTT GGG CGT CGC TTG GTC GGT CAT TTC GAA CCC CAG AGT CC
R1^{100}	GGA CTC TGG GGT TCG AAA TGA CCG ACC AAG CGA CGC CCA ACC TGC CAT CAC GAG ATT TCG ATT CCA CCG CCG CCT TCT ATG AAA GGT TGG GCT TCG GAC C
R2^{100}	GGT CCG AAG CCC AAC CTT TCA TAG AAG GCG GCG GTG GAA TCG AAA TCT CGT GAT GGC AGG TTG GGC GTC GCT GGT CGT CAT TCG AAC CCC AGA GTC C
D1^{38}	DBCO-ATCAACACTGCACACCAGACAGCAAGATCCTATATATA
D2^{38}	Alexa 647-TATATATAGGATCTTGCTGTCTGGTGTGCAGTGTTGAT
D1^{50}	TAT CAG TAG GTT CTT CAG AGT ATT GTC TCT TCC GTG TAT CAG TTA GCC TC-DBCO
D2^{50}	Alexa 647-GAG GCT AAC TGA TAC ACG GAA GAG ACA ATA CTC TGA AGA ACC TAC TGA TA
D1^{100}	TAT CAG TAG GTT CTT CAG AGT ATT GTC TCT TCC GTG TAT CAG TTA GCC TCG ACT CTC ATA GTG GAC GTA GAA CTC CAC ATC AGA TCA CTG GAA GAT CAT C-DBCO
D2^{100}	Alexa 647-GAT GAT CTT CCA GTG ATC TGA TGT GGA GTT CTA CGT CCA CTA TGA GAG TCG AGG CTA ACT GAT ACA CGG AAG AGA CAA TAC TCT GAA GAA CCT ACT GAT A
BIOTIN-R-CELL	Biotin-AAA ATA CAT TTA TAT ATA TCC TAG TCC GAC CGC AGG ATC CTA TAA
R-CELL	TAC ATT TAT ATA TAT CCT AGT CCG ACC GCA GGA TCC TAT AA
BIOTIN-O3-CELL	TTA TAG GAT CCT GCG GTC GGA CTA GGA TAT ATA TAA ATG TAA AAA-Biotin
O3-CELL	TTA TAG GAT CCT GCG GTC GGA CTA GGA TAT ATA TAA ATG TA
R1-CELL	TTA TAG GAT CCT GCG GT
RM-CELL	GCG GTC GGA CTA GGA TA
R2-CELL	GGA TAT ATA TAA ATG TA
R3-CELL	AGG ATC CTG CGG TCG GA
R4-CELL	TCC TGC GGT CGG ACT AG
R5-CELL	GCG GTC GGA CTA GGA TA
BIOTIN-RR6-CELL	Biotin-AAA ATA CAT TTA TAT ATA TCC TAG TCC ATA GAC CGC AGG ATC CT
R6-CELL	AGG ATC CTG CGG TCT TAT GGA CTA GGA TAT ATA TAA ATG TA
BIOTIN-R-CELL-33	Biotin-AAAATACATTTCCTAGTCCGACCGCAGGATCCTATAA
O3-CELL-33	TTATAGGATCCTGCGGTCGGACTAGGAAATGTA
BIOTIN-DS1-CELL	Biotin-AAA ATG CAG GGT ACG GTA CGG TAC GCC GGA CGC GAC TAG TTA CGG
DS2-CELL	CCG TAA CTA GTC GCG TCC GGC GTA CCG TAC CGT ACC CTG CA
I4-CELL	CCC CTA ACC CCT AAC CCC TAA CCC CAT ATA TAT CCT AGA ACG ACA GAC AAA CAG TGA TAA
I4-COMP-CELL	TTA TCA CTG TTT GTC TGT CGT TCT AGG ATA TAT ATT TTG TTA TGT GTT ATG TGT TAT
nD'	AT CAA CAC TGC ACA CCA GAC AGC TAG GAT CCT ATA A
nD^{647}	TTA TAG GA/iATTO647NN/ CCT AGC TGT CTG GTG TGC AGT GTT GAT
nD'^{488}	Alexa488-AT CAA CAC TGC ACA CCA GAC AGC TAG GAT CCT ATA A
nD'-9E	TCA CAC TGC ACA CTA CAG ACA GCA AGA TCCA
nD^{647N}-9E	TGGA TCT TGC TGT CTG TAG TGT GCA GTG TGA
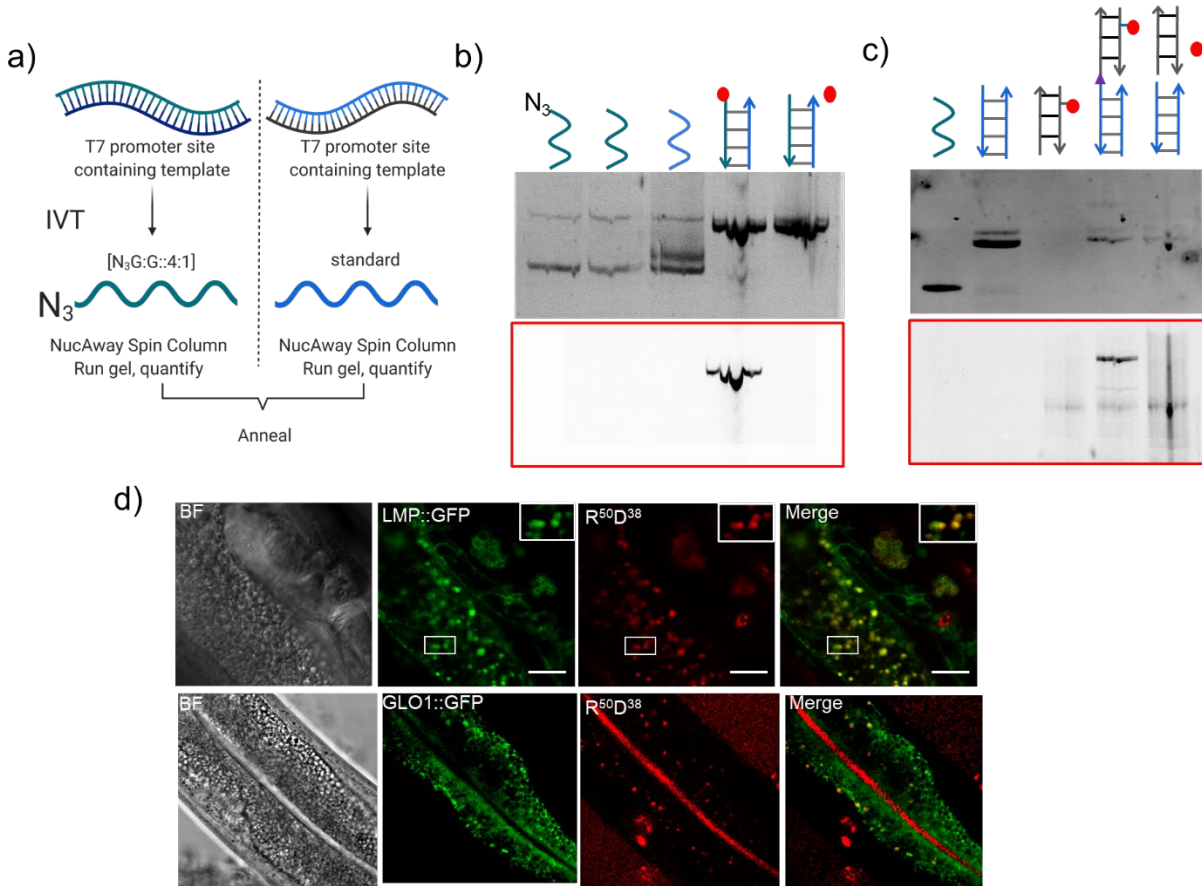
Supplementary Fig1: Uptake of nucleic acid probes in the intestinal epithelial cells a) Schematic showing protocol of synthesis of azide labelled RNA for R^{50} and R^{100} strands. b) The conjugation of Alexa 647N was confirmed by gel electrophoresis for R^{50}. The 8% Native PAGE gel was imaged in the EtBr channel and Alexa 647N channel (red box). c) The conjugation of R^{100} (lane 2) with D^{38} (lane 3) to form $R^{100}D^{38}$ (lane 4) was confirmed by gel electrophoresis. The 15% Native PAGE gel was imaged in the EtBr channel. d) Representative images of colocalization between LRO markers (LMP1::GFP and GLO-1::GFP) and $R^{100}D^{38}$ fluorophore labeled nucleic acid probes in intestinal epithelial cells.

To test whether our R^nD^n devices localized in LROs we performed colocalization experiments in transgenic worms expressing fluorescently labelled lysosomal markers LMP1::GFP or GLO-1::GFP that label lysosomes and LROs respectively. The transgenics were incubated in a solution of 1 µM $R^{100}D^{38}$ for 2 h. Worms were then washed and incubated on OP50 plates for 1 hour for clearing their intestine lumens of excess $R^{100}D^{38}$. Our experiments revealed that $R^{100}D^{38}$ and LMP1::GFP showed high colocalization, indicating that the nanodevices labeled LROs. Similarly $R^{100}D^{38}$ and GLO-1::GFP also colocalized. However, there was lower uptake into the IEC's and poorer clearance of the gut lumen in GLO-1::GFP transgenic worms.
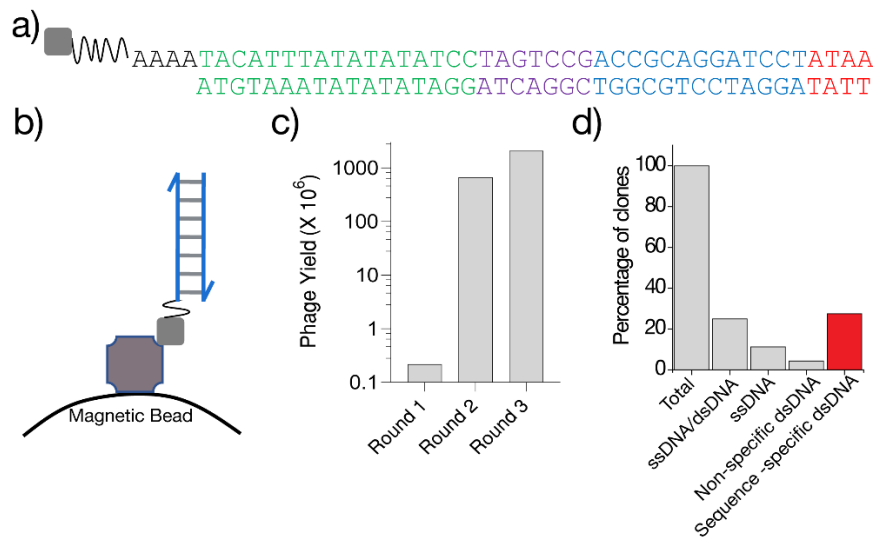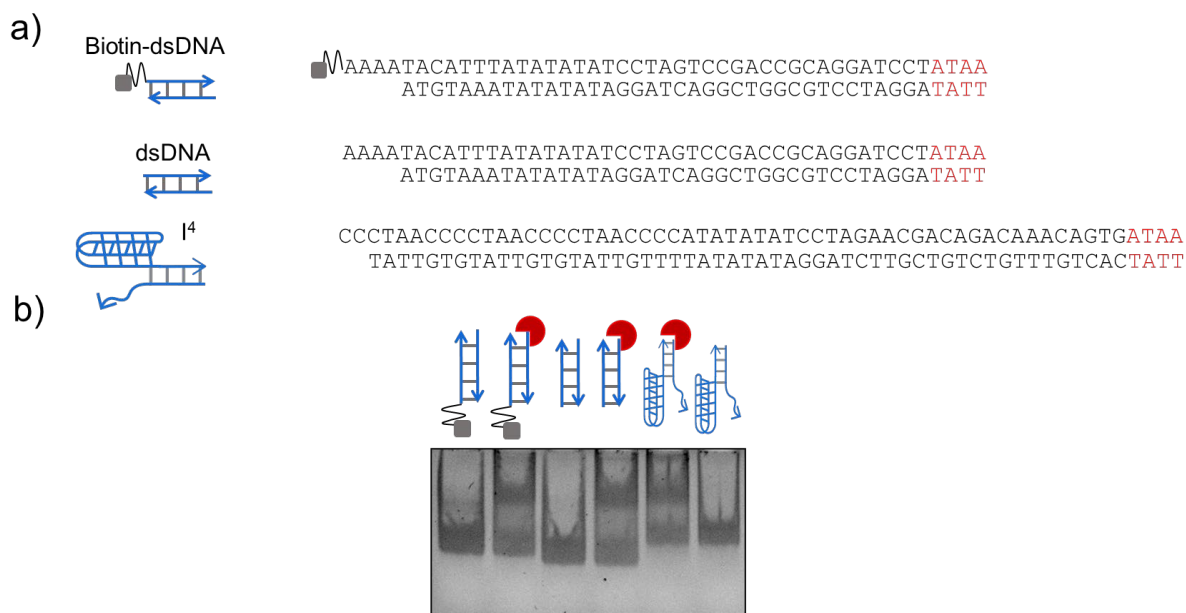
Supplementary Figure 2: Analysis of recombinant antibody binders of a dsDNA epitope. a) Sequence of the biotin-labeled dsDNA epitope used for the phage display screen. b) The epitope was immobilized via biotin (grey square) on streptavidin conjugated magnetic beads. c) Yield of the phages after each round of selection, calculated as described in Materials and Methods. d) Percentage of V_HH clones obtained that bound the indicated epitope and their sequence specificity.
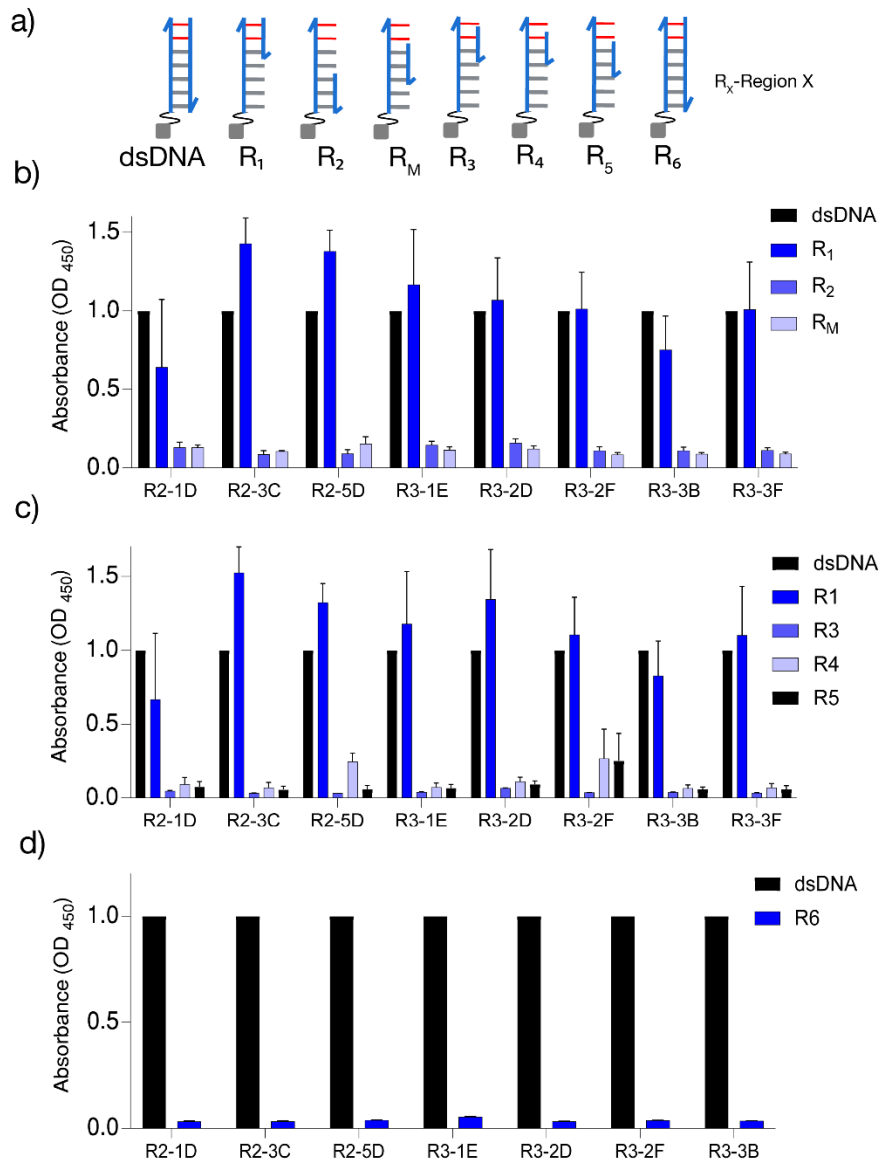
Supplementary Figure 3: Characterization of dsDNA-binding V_HH antibodies. a) Schematic of the dsDNA constructs used to find the minimal dsDNA-binding motif. All sequence details are provided in Supplementary Table 1. Epitopes were immobilized on streptavidin conjugated magnetic beads via biotin (grey square). Relative binding of a few representative dsDNA-binding V_HH antibodies to b) duplexes R_1, R_2 and R_M, c) duplexes R_3, R_4 and R_5, d) duplex R_6. All ELISA experiments were performed in triplicate and errors are presented as mean ± s.e.m.
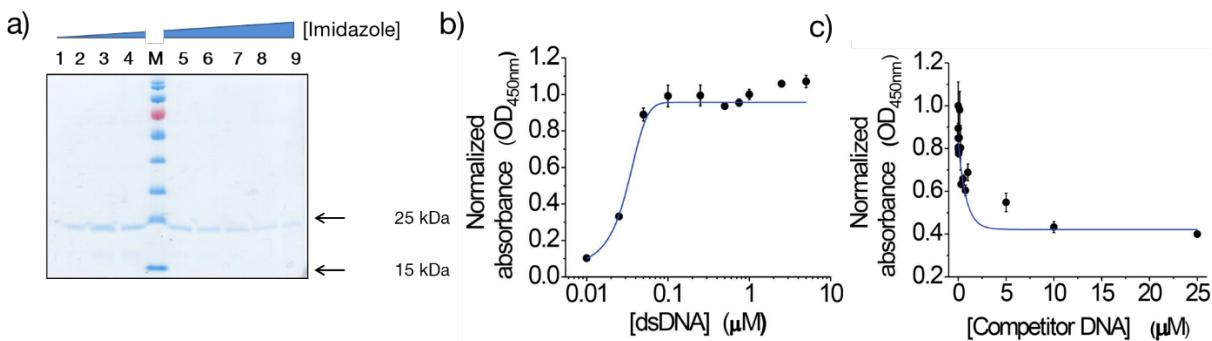
Supplementary Figure 4: a) Purification of the dsDNA-binding 9E. Clone 9E was expressed and purified as described in Materials and Methods, and the fractions obtained after elution using increasing concentrations of imidazole were resolved on a 12.5% SDS-polyacrylamide gel. Fractions 3-9 were found to be enriched in the eluted protein. Semi-quantitative determination of affinity of 9E for the 41-mer dsDNA using (b) increasing concentrations of immobilized dsDNA and fixed amount of protein (250 nM), and (c) immobilized dsDNA (500 nM) in the presence of increasing amounts of competitor dsDNA. All experiments were performed in triplicate and the data is represented as mean ± s.e.m.

a)

Biotin-dsDNA

AAAATACATTTATATATATCCTAGTCCGACCGCAGGATCCTATAA
ATGTAAATATATATAGGATCAGGCTGGCGTCCTAGGATATT

dsDNA

AAAATACATTTATATATATCCTAGTCCGACCGCAGGATCCTATAA
ATGTAAATATATATAGGATCAGGCTGGCGTCCTAGGATATT

I^4

CCCTAACCCCTAACCCCTAACCCCATATATATCCTAGAACGACAGACAAACAGTGATAA
TATTGTGTATTGTGTATTGTTTTATATATAGGATCTTGCTGTCTGTTTGTCACTATT

b)

Supplementary Figure 5. Electrophoretic mobility shift assay (EMSA) to demonstrate binding of 9E to the 4 nt minimal binding motif. (a) Sequences, and the corresponding schematics, of DNA constructs engineered with the 4 nt epitope (red) to demonstrate binding of 9E. (b). EMSA of 9E (red crescent) to biotinylated dsDNA (lanes 1, 2), dsDNA (lanes 3, 4) and a DNA duplex (I^4; lanes 5, 6) where the 4 nt epitope was placed at one end of the duplex (region highlighted in red), while the other end comprised an I-motif forming C-rich segment. Binding assays were set up as described in Materials and Methods and run on an 8% non-denaturing polyacrylamide-TAE gel.
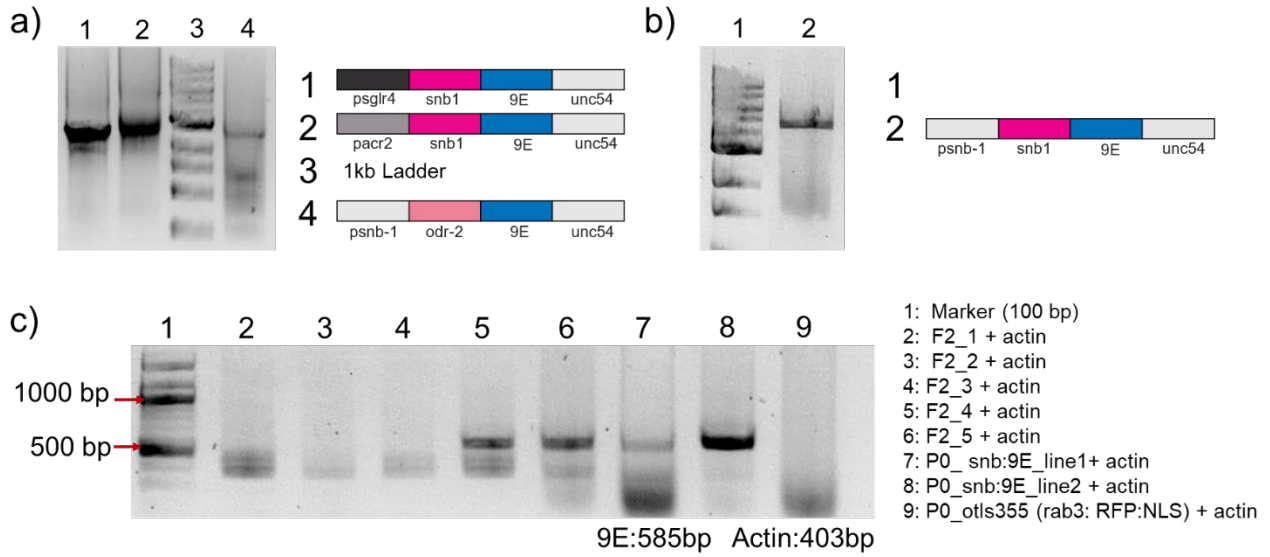
Supplementary Figure 6: a) and b) PCR fragments used for making various transgenic strains to target DNA probes to neurons. PCR product was confirmed by gel electrophoresis with 1% Agarose gel and c) single worm PCR showing selection of worms containing p*snb-1:snb-1:: 9E* and 2XNLS::RFP
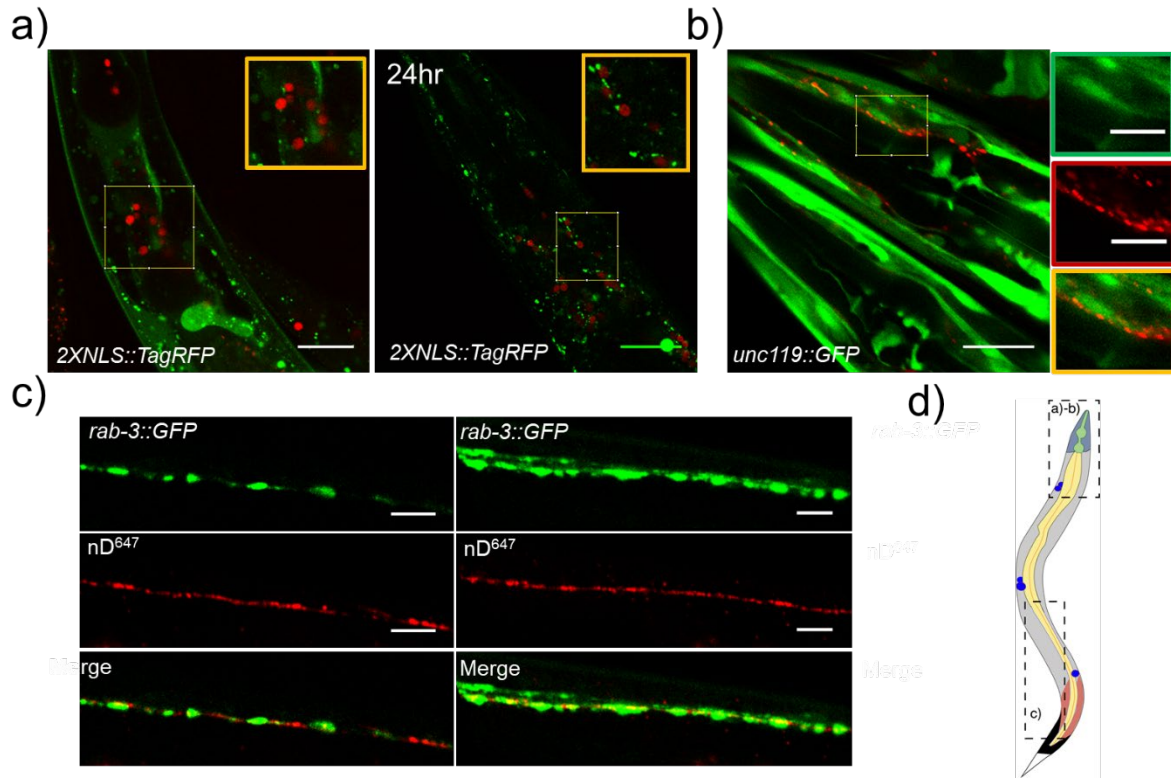
Supplementary Figure 7: Schematic showing selection of worms containing psnb-1:snb-1:: 9E and 2XNLS::RFP: Representative merged images of transgenic worms containing both a) *rab-3p(prom1)::2xNLS::TagRFP* or b) *unc-119::GFP* or c) *prab-3::gfp::rab-3* and *psnb-1:snb-1::9E* injected with nDNA. d) Schematic showing regions of the worm represented in a-c. Scale bar a) 20 μm; b) 20 μm, inset- 5μm and c) 5μm.

Bibliography

1. Paredes, E. & Das, S. R. Click chemistry for rapid labeling and ligation of RNA. *Chembiochem* **12,** 125–131 (2011).

2. Jewett, J. C., Sletten, E. M. & Bertozzi, C. R. Rapid Cu-free click chemistry with readily synthesized biarylazacyclooctynones. *J. Am. Chem. Soc.* **132,** 3688–3690 (2010).

3. Baskin, J. M. *et al.* Copper-free click chemistry for dynamic in vivo imaging. *Proc. Natl. Acad. Sci. USA* **104,** 16793–16797 (2007).

4. Milligan, J. F., Groebe, D. R., Witherell, G. W. & Uhlenbeck, O. C. Oligoribonucleotide synthesis using T7 RNA polymerase and synthetic DNA templates. *Nucleic Acids Res.* **15,** 8783–8798 (1987).

5. Huang, F., He, J., Zhang, Y. & Guo, Y. Synthesis of biotin-AMP conjugate for 5' biotin labeling of RNA through one-step in vitro transcription. *Nat. Protoc.* **3,** 1848–1861 (2008).

6. Merritt, C., Rasoloson, D., Ko, D. & Seydoux, G. 3' UTRs are the primary regulators of gene expression in the C. elegans germline. *Curr. Biol.* **18,** 1476–1482 (2008).

7. Brenner, S. Caenorhabdztzs elegans. 71–94 (1974).

8. Mahoney, T. R. *et al.* Regulation of synaptic transmission by RAB-3 and RAB-27 in Caenorhabditis elegans. *Mol. Biol. Cell* **17,** 2617–2625 (2006).

9. Bounoutas, A., Zheng, Q., Nonet, M. L. & Chalfie, M. mec-15 encodes an F-box protein required for touch receptor neuron mechanosensation, synapse formation and development. *Genetics* **183,** 607–17, 1SI (2009).

10. Nguyen, J. P. *et al.* Whole-brain calcium imaging with cellular resolution in freely behaving Caenorhabditis elegans. *Proc. Natl. Acad. Sci. USA* **113,** E1074–81 (2016).

11. Altun-Gultekin, Z. *et al.* A regulatory cascade of three homeobox genes, ceh-10, ttx-3 and ceh-23, controls cell fate specification of a defined interneuron class in C. elegans. *Development* **128,** 1951–1969 (2001).

12. Treusch, S. *et al.* Caenorhabditis elegans functional orthologue of human protein h-mucolipin-1 is required for lysosome biogenesis. *Proc. Natl. Acad. Sci. USA* **101,** 4483–4488 (2004).

13. Zhang, S. O., Trimble, R., Guo, F. & Mak, H. Y. Lipid droplets as ubiquitous fat storage organelles in C. elegans. *BMC Cell Biol.* **11,** 96 (2010).

14. Mello, C. C., Kramer, J. M., Stinchcomb, D. & Ambros, V. Efficient maintenance. **10,** 3959–3970 (1991).

15. Granato, M., Schnabel, H. & Schnabel, R. *pha-1* , a selectable marker for gene transfer in*C.elegans*. *Nucleic Acids Res.* **22,** 1762–1763 (1994).

16. Stinchcomb, D. T., Shaw, J. E., Carr, S. H. & Hirsh, D. Extrachromosomal DNA transformation of Caenorhabditis elegans. *Mol. Cell. Biol.* **5,** 3484–3496 (1985).

17. Single worm PCR | Schedl Lab. at <http://genetics.wustl.edu/tslab/protocols/genomic-stuff/single-worm-pcr/>

18. Sauvola, J. & Pietikäinen, M. Adaptive document image binarization. *Pattern Recognit* **33,** 225–236 (2000).